AGU PUBLICATIONS

Tectonics

RESEARCH ARTICLE
10.1002/2015TC003918

Key Points:
- The Grant Range exhibits brittle faulting at dips of 15° or less
- A "fixed hinge" model of stationary flexural isostatic uplift is proposed
- Excision is observed both updip and downdip of the axis of uplift

Supporting Information:
- Texts S1–S6, Figures S1–S3, and Tables S1–S6

Correspondence to:
S. P. Long,
sean.p.long@wsu.edu

Citation:
Long, S. P., and J. P. Walker (2015), Geometry and kinematics of the Grant Range brittle detachment system, eastern Nevada, U.S.A.: An end-member style of upper crustal extension, *Tectonics*, *34*, 1837–1862, doi:10.1002/2015TC003918.

Received 1 MAY 2015
Accepted 1 AUG 2015
Accepted article online 6 AUG 2015
Published online 17 SEP 2015

Geometry and kinematics of the Grant Range brittle detachment system, eastern Nevada, U.S.A.: An end-member style of upper crustal extension

Sean P. Long[1,2] and Jerome P. Walker[3]

[1]Nevada Bureau of Mines and Geology, University of Nevada, Reno, Nevada, USA, [2]Now at School of the Environment, Washington State University, Pullman, Washington, USA, [3]Reno, Nevada, USA

Abstract Documenting the range of styles of normal faulting is fundamental to understanding crustal extension. Here geologic mapping, field relationships, and deformed and restored cross sections illustrate the geometry and kinematic development of a system of west-vergent detachment faults in the Grant Range in eastern Nevada. Faults exhibit brecciation and stratigraphic cutoff angles of 5–15° at all structural levels and deform a 10 km thick section of Paleozoic and Paleogene rocks. The fault system is folded across an anticlinal culmination, which grew during extension, as indicated by progressively increasing interlimb angles and incision in the axial zone. The eastern limb consists of an imbricate stack of faults that were emplaced from bottom to top. In the western limb, several faults exhibit apparent thrust relationships. The oldest faults are cut by a ~29 Ma dike, and the highest preserved fault cuts ~32 Ma volcanic rocks that restore to paleodepths of ~1 km. Retrodeformation of folding and minimal structural relief and angularity across a Paleogene unconformity indicate the faults were active at 5–15° angles. Retrodeformation of offset indicates ≥49 km (98%) extension. We propose a model of stationary, sustained isostatic uplift and incision at the culmination axis (a "fixed hinge"), with updip excision producing bottom-to-top growth of the imbricate stack and downdip excision producing apparent thrust relationships. The fault system exhibits similarities to core complex detachment systems, though it is confined to upper crustal levels, and there are no preserved high-angle or listric normal faults, indicating a unique extension style dominated by low-angle excision.

1. Introduction

Continental extension at upper crustal levels is accommodated by brittle normal faults with a wide range of geometries [e.g., *Proffett*, 1977; *Lister and Davis*, 1989; *Burchfiel et al.*, 1992; *Stewart*, 1998; *Axen*, 2007; *Kapp et al.*, 2008], and documenting the variability in styles of normal faulting is fundamental to understanding how the crust responds during extensional tectonism. In continental rift settings such as the Basin and Range province, upper crustal extension is most commonly accommodated by systems of normal faults that initially develop at a high angle (~60–70°), such as spaced systems that form half-graben geometries [e.g., *Nur et al.*, 1986; *Stewart*, 1998] or closely spaced arrays of faults that undergo domino-style rotation with progressive extension [e.g., *Proffett*, 1977; *Chamberlin*, 1983; *Brady et al.*, 2000]. In contrast, upper crustal extension has also been documented along normal faults that originated at dips ≤30° [e.g., *Yin and Dunn*, 1992; *Wernicke*, 1995; *Axen*, 2004], which are referred to here as detachment faults. Slip at such low angles continues to be a debated and highly polarized subject, due to mechanical theory that predicts only steep (~60°) seismogenic normal faulting [*Anderson*, 1942], and sparse evidence for modern seismicity at shallow dip angles [e.g., *Jackson and White*, 1989; *Collettini and Sibson*, 2001]. However, despite these unresolved debates, detachment faults continue to be identified globally, in a variety of tectonic settings, including metamorphic core complexes [e.g., *Davis and Coney*, 1979; *Crittenden et al.*, 1980; *Wernicke*, 1981; *Lister and Davis*, 1989], within active and ancient contractional orogens [e.g., *Dalmayrac and Molnar*, 1981; *Selverstone*, 1988; *Burchfiel et al.*, 1992; *Wells et al.*, 2012], within nonvolcanic passive margins [e.g., *Lister et al.*, 1986; *Abers*, 2001; *Boillot and Froitzheim*, 2001], and at mid-ocean ridges [e.g., *Tucholke and Lin*, 1998; *Hansen et al.*, 2013].

Within metamorphic core complexes, high-magnitude extension results in localization of strain along large-offset detachment systems, and several aspects of the structural evolution of these systems remain

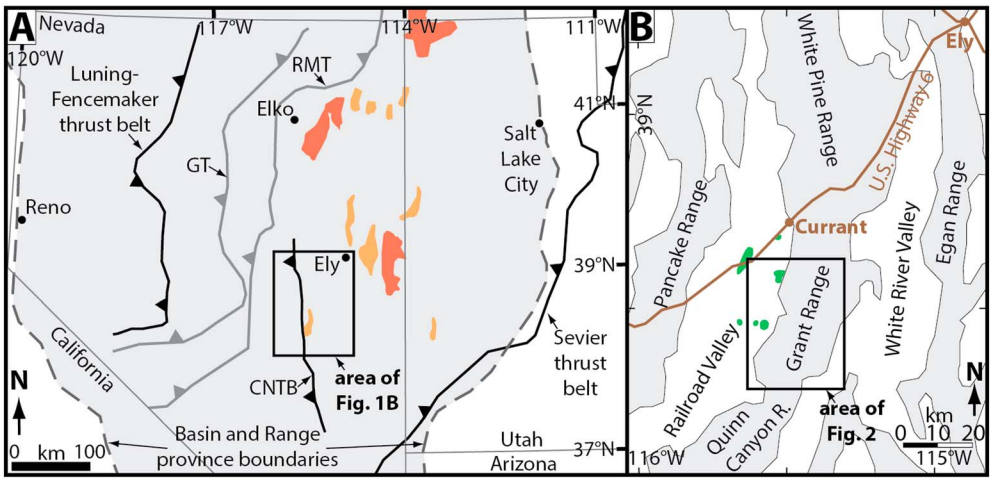

Figure 1. (a) Map of Nevada and western Utah; deformation fronts of Paleozoic thrust systems (GT = Golconda thrust; RMT = Roberts Mountains thrust) shown in dark gray, and deformation fronts of Mesozoic thrust systems (CNTB = Central Nevada thrust belt) shown in black [modified from *Long et al.*, 2014]. Area of Basin and Range province is shaded light gray [from *Dickinson*, 2006]. Areas of exposed Mesozoic metamorphic rocks are highlighted, including metamorphic core complexes in red and highly extended ranges in orange [locations from *Miller and Gans*, 1989; *Camilleri and Chamberlain*, 1997]. (b) Map showing location of Grant Range and geographic names of surrounding ranges and valleys. Railroad Valley oil fields highlighted in green [locations from *Peterson*, 1994].

controversial [e.g., *Wernicke and Axen*, 1988; *Livaccari et al.*, 1995; *Axen*, 2007]. One debate centers on the role of denudation-induced isostatic rebound in tilting detachment faults to progressively shallower dip angles. This process was initially called upon to dome and rotate detachment systems that were active at shallow (≤30°) angles [*Spencer*, 1984] and was later proposed to significantly rotate seismogenic normal faults originally active at high angles (up to 60°) to the gentle dips observed today (the "rolling hinge" model) [*Buck*, 1988; *Wernicke and Axen*, 1988]. Another debate centers on the style of normal faulting in the complexly extended, upper plate sections of core complex detachment systems, and how upper plate extension relates geometrically to the basal detachment [e.g., *Lister and Davis*, 1989]. Upper plate extension is commonly interpreted to be accommodated by arrays of listric normal faults that sole into the basal detachment [e.g., *Davis et al.*, 1980] or by sets of high-angle, domino-style normal faults that progressively rotate and feed offset into the basal detachment [e.g., *Gans and Miller*, 1983].

To contribute to these debates, we present a case study from the Grant Range in eastern Nevada (Figure 1), which contains an exceptionally well-exposed system of brittle detachment faults [e.g., *Lund et al.*, 1993]. We integrate geologic mapping in a transect across the range with analysis of the geometries and crosscutting relations of detachment faults, lithologic logs and attitude data from oil wells, deformed and restored cross sections, and $^{40}Ar/^{39}Ar$ geochronology, to present a model for the geometric and kinematic development of this fault system. The Grant Range fault system exhibits several geometric similarities to core complex detachment systems, but exposed levels are confined to the upper ~10 km of the crust. However, superbly exposed field relations and several aspects of the kinematic development of the fault system make the Grant Range a unique natural laboratory for analyzing primary fault slip angles, for testing models for the magnitude and style of synextensional, isostatic flexural rotation, and for understanding the range in styles of internal extension of upper plate rocks in core complex-type fault systems.

2. Regional Tectonic Framework

From the Neoproterozoic to the Devonian, eastern Nevada occupied a passive margin setting, where shallow marine clastic and carbonate rocks were deposited on the western Laurentian continental shelf [e.g., *Stewart and Poole*, 1974]. During the Late Devonian-Mississippian Antler orogeny, deep-marine clastic rocks were accreted above the east-vergent Roberts Mountains thrust (Figure 1a), producing contemporary deposition in a foreland basin in eastern Nevada [e.g., *Poole and Sandberg*, 1977; *Speed and Sleep*, 1982]. Following the

Antler orogeny, shallow marine deposition of dominantly carbonate rocks resumed in eastern Nevada from the Pennsylvanian to the Triassic [e.g., *Stewart*, 1980], interrupted by localized uplift and erosion events [e.g., *Trexler et al*., 2004; *Cashman et al*., 2011].

During the Jurassic to Paleogene Cordilleran orogenic event, eastern Nevada lay in the hinterland of the Sevier thrust belt [e.g., *Armstrong*, 1968; *DeCelles*, 2004] (Figure 1a). In the Sevier hinterland, low-magnitude upper crustal shortening was accommodated by the central Nevada thrust belt [*Taylor et al*., 2000; *Long*, 2012] (Figure 1a) and by regional-scale, open folding across eastern Nevada [*Gans and Miller*, 1983; *Long*, 2015]. Though upper crustal shortening was minor, ductile deformation and metamorphism occurred at midcrustal levels, often associated spatially with Jurassic and Late Cretaceous granitic plutonism [*Miller et al*., 1988; *Miller and Gans*, 1989; *Barton*, 1990; *Miller and Hoisch*, 1995; *Wells and Hoisch*, 2008]. These metamorphic rocks are now exposed in a series of core complexes and highly extended ranges in eastern Nevada and western Utah (Figure 1a).

During the Late Cretaceous and Paleogene, eastern Nevada has been interpreted as an orogenic plateau [e.g., *Coney and Harms*, 1984; *Allmendinger*, 1992; *DeCelles*, 2004]. Evidence for spatially localized Late Cretaceous and Paleogene extension in this plateau, including exhumation of midcrustal rocks now exposed in metamorphic core complexes [e.g., *Hodges and Walker*, 1992; *Lewis et al*., 1999; *McGrew et al*., 2000; *Wells and Hoisch*, 2008] and upper crustal normal faulting [e.g., *Taylor et al*., 1989; *Gans et al*., 1989, 2001; *Vandervoort and Schmitt*, 1990; *Axen et al*., 1993; *Camilleri and Chamberlain*, 1997; *Druschke et al*., 2009a, 2009b; *Long et al*., 2015], records a protracted, spatially heterogeneous transition to an extensional tectonic regime in eastern Nevada. However, the inception of widespread extension that formed the Basin and Range province (Figure 1a), which is attributed to reorganization of the Pacific-North American plate boundary [e.g., *Atwater*, 1970], was not until the middle Miocene [e.g., *Dickinson*, 2002, 2006; *Colgan and Henry*, 2009].

3. Grant Range Stratigraphic and Structural Setting

Physiographically, the Grant Range lies between Railroad Valley to the west and White River Valley to the east and adjoins the White Pine Range to the north and the Quinn Canyon Range to the south (Figures 1b and 2).

Paleozoic rocks exposed in the Grant Range consist of 8–10 km of Cambrian to Pennsylvanian carbonate and clastic rocks; readers are referred to *Moores et al*. [1968], *Fryxell* [1988], *Camilleri* [2013], and *Long* [2014] for detailed unit descriptions. In the study area, which lies in the central Grant Range (Figure 2), a 7 km thick section of Cambrian to Pennsylvanian rocks is exposed, and is dominated by limestone and dolomite, with lesser sandstone and shale (Figure 3). Stratigraphic divisions for Cambrian and Ordovician rocks differ in previous studies [*Lund et al*., 1987, 1988, 1993; *Fryxell*, 1988; *Camilleri*, 2013]; in this study, divisions defined by *Camilleri* [2013] were used.

Cambrian and Ordovician rocks in the Grant Range record a history of Mesozoic metamorphism and magmatism [e.g., *Fryxell*, 1988; *Taylor et al*., 2000; *Camilleri*, 2013] (Figure 2). Greenschist facies metamorphism has produced low-grade metasedimentary lithologies, including phyllitic marble and micaceous limestone from carbonate protoliths, quartzite from sandstone protoliths, and phyllite from shale protoliths. In the study area, initial metamorphism accompanied mesoscale, east-vergent folding and development of axial-planar cleavage, followed by a stage of static, peak metamorphism and a second stage of synkinematic metamorphism accompanying mesoscale, west-vergent folding [*Camilleri*, 2013]. In the southern Grant Range, the Troy granite stock intruded Cambrian stratigraphic levels [*Fryxell*, 1988] (Figure 2). U-Pb zircon geochronology reveals a Jurassic age (~163 Ma) for boudinaged granite sills on the western margin of the stock and a Late Cretaceous age (~84 Ma) for undeformed granite that forms the bulk of the pluton, indicating multiple emplacement ages [*Lund et al*., 2014]. Peak metamorphism of Cambrian and Ordovician rocks is interpreted to have been contemporary with intrusion of the Late Cretaceous component of the stock [*Fryxell*, 1988; *Lund et al*., 1993; *Camilleri*, 2013].

In the Quinn Canyon Range and southern Grant Range, east-vergent thrust faults deform Cambrian through Devonian rocks (Figure 2) [*Fryxell*, 1988; *Bartley and Gleason*, 1990; *Taylor et al*., 2000]. These faults are correlated with the central Nevada thrust belt, a series of Mesozoic thrust faults that connect southward with the Sevier thrust belt (Figure 1a) [*Taylor et al*., 2000; *Long*, 2012]. However, in the central and northern

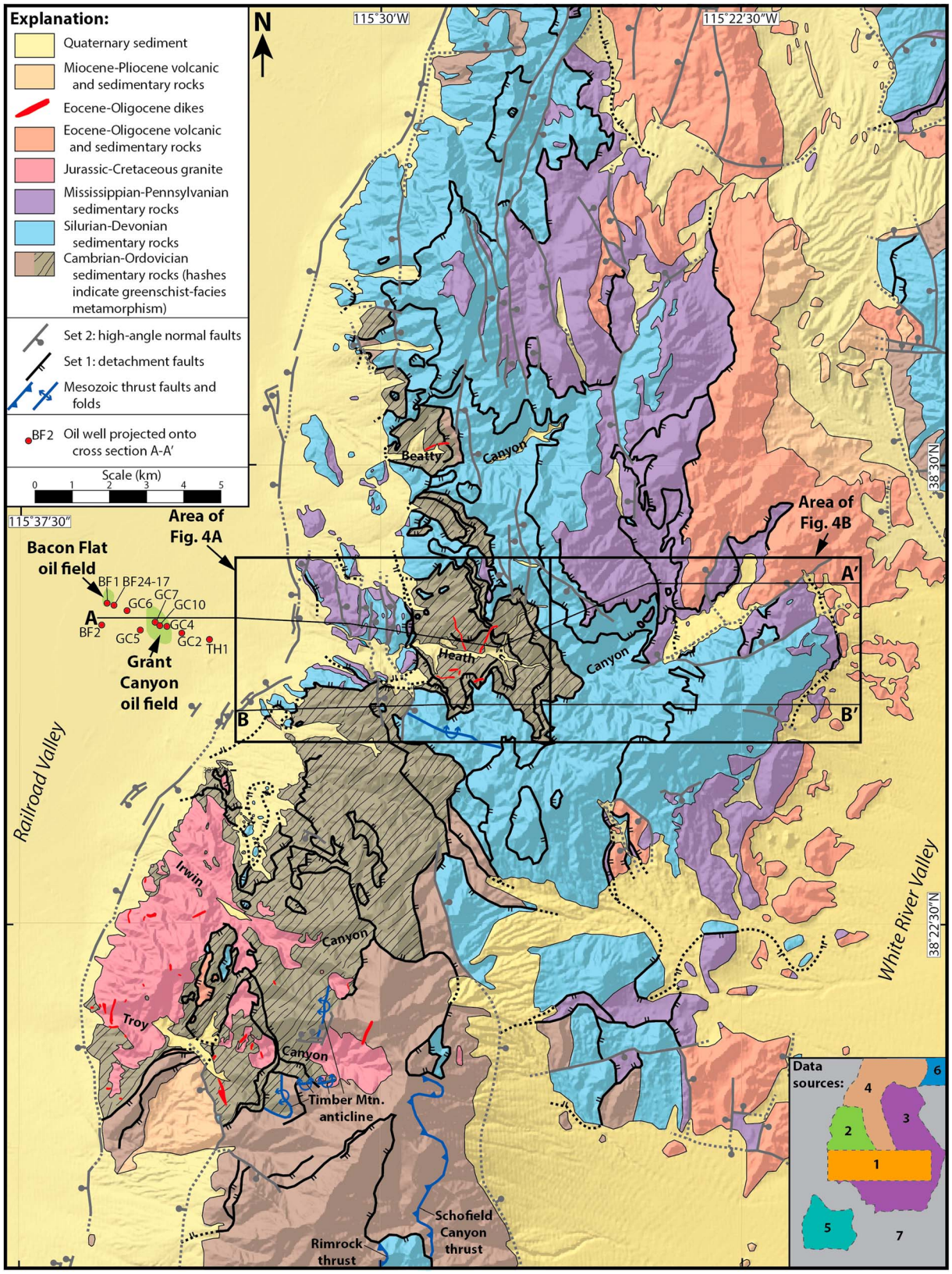

Figure 2. Simplified geologic map of the central and southern Grant Range, compiled from the following mapping sources (see lower right inset): 1 = *Long* [2014]; 2 = *Camilleri* [2013]; 3 = *Lund et al.* [1988]; 4 = *Lund et al.* [1987]; 5 = *Fryxell* [1988]; 6 = *Moores et al.* [1968]; 7 = *Kleimhampl and Ziony* [1985]. Oil well locations from *Hess et al.* [2004].

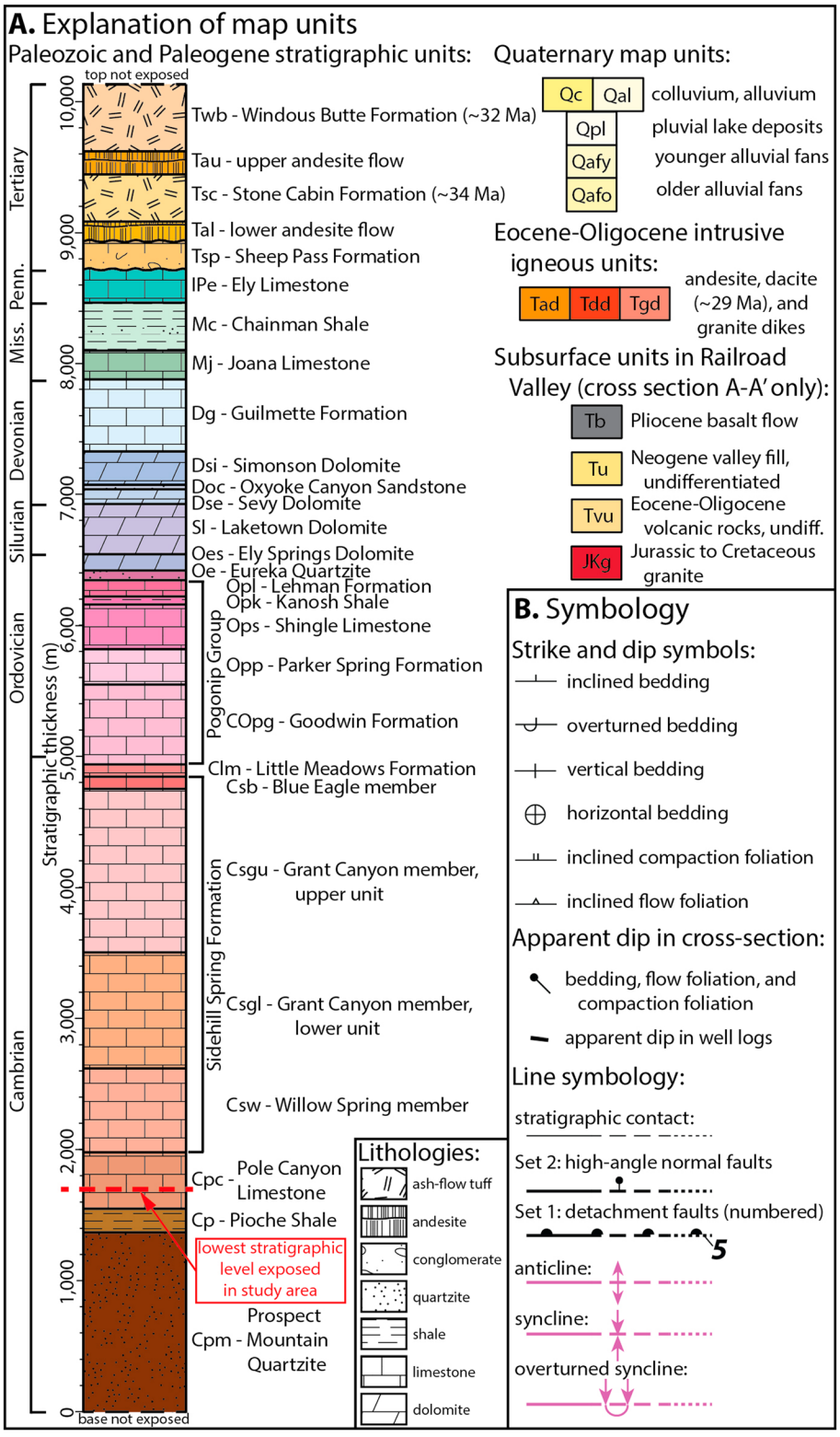

Figure 3. (a) Guide to lithologies, stratigraphic thicknesses, and abbreviations of map units shown in Figures 4–6. Ages for Stone Cabin Formation from *Kleimhampl and Ziony* [1985] and Windous Butte Formation from *Taylor et al.* [1989]; ~29 Ma age of dacite dike (map unit Tdd) from this study (supporting data in the supporting information). (b) Guide to symbology of map and cross sections shown in Figures 4–6.

Grant Range, regionally continuous, older-over-younger relationships indicative of macroscale thrust faults have not been documented through the exposed Cambrian to Pennsylvanian section [*Moores et al*., 1968; *Lund et al*., 1987, 1988, 1993].

Paleozoic rocks are unconformably overlain, at Mississippian to Pennsylvanian erosion levels, by Paleogene sedimentary and volcanic rocks. Conglomerate and limestone of the Paleocene-Eocene Sheep Pass Formation [*Fouch*, 1979] are regionally interpreted to represent deposition within half-grabens [*Kellogg*, 1964; *Vandervoort and Schmitt*, 1990; *Druschke et al*., 2009a]. Late Eocene to Oligocene silicic volcanic rocks of the Great Basin ignimbrite flare-up [e.g., *Armstrong and Ward*, 1991; *Best and Christiansen*, 1991], which consist dominantly of rhyolitic ash flow tuffs, with less common andesite and rhyolite flows, in places exhibit cumulative thicknesses of ~1700–2000 m [*Moores et al*., 1968; *Taylor et al*., 1989]. In the study area, the ~34.1 Ma (K-Ar biotite) [*Kleimhampl and Ziony*, 1985] Stone Cabin Formation is the oldest volcanic unit exposed, and the ~31.8 Ma (^{40}Ar/^{39}Ar biotite) [*Taylor et al*., 1989] Windous Butte Formation is the youngest (Figure 3).

Paleozoic and Paleogene rocks in the central and northern Grant Range are deformed by a system of low dip angle, low stratigraphic cutoff angle, top-down-to-west detachment faults (Figure 2) [*Camilleri*, 1992, 2013; *Lund et al*., 1993], referred to here as set 1 faults, which are the subject of this paper. On the east side of the range, set 1 faults cut volcanic units as young as Oligocene (Figure 2) [*Lund et al*., 1988]. However, set 1 faults in the western part of the range are cut by dikes of presumed Eocene-Oligocene age (Figure 2) [*Camilleri*, 2013; *Long*, 2014], including a ~29 Ma (^{40}Ar/^{39}Ar biotite; supporting data in the supporting information) dacite dike dated in this study (sample GR63, Figure 4), indicating that set 1 extension had to have begun by the late Oligocene.

Throughout the Grant Range, high-angle normal faults of variable strike and dip direction cut set 1 faults and do not reactivate them (Figures 2 and 4) [*Moores et al*., 1968; *Lund et al*., 1987, 1988, 1993; *Camilleri*, 2013; *Long*, 2014], indicating that they represent one or more distinctly younger episodes of extension. They are classified here as set 2 faults, a definition which also includes faults associated with formation of the Railroad Valley structural basin, including the west dipping, range-bounding fault system which exhibits scarps that cut Quaternary alluvial fans (Figure 4) [*Camilleri*, 2013; *Long*, 2014]. In the northern Grant Range, the middle-late Miocene [~16–9 Ma; *Horton and Schmitt*, 1998] Horse Camp Formation is exposed and is interpreted to have been deposited during a period of major extension [*Moores et al*., 1968; *Horton and Schmitt*, 1998]. The Railroad Valley structural basin, which is bound on the east by a master, west dipping fault system, contains up to 3000 m of late Miocene to Holocene valley fill sediment (Figure 5a) [*Johnson*, 1993]. The basal valley fill section is time equivalent to the lower Horse Camp Formation, defining contemporary early development of Railroad Valley and the Horse Camp basin [*Johnson*, 1993; *Horton and Schmitt*, 1998]. Basalt flows in the upper part of the valley fill section (Figure 5a) are correlative with Pliocene and younger flows along the western margin of Railroad Valley [*Kleimhampl and Ziony*, 1985; *Johnson*, 1993; *Hulen et al*., 1994].

4. Geologic Map and Cross Sections

Geologic mapping of a 20 km wide transect across the central Grant Range (Figure 2) was performed at 1:24,000 scale [*Long*, 2014] and is presented on Figure 4 at ~1:37,250. The mapping was used to support drafting of cross sections A–A′ (Figure 5a) and B–B′ (Figure 6a), which are oriented approximately parallel to the overall east-west extension direction [e.g., *Lund et al*., 1993; *Camilleri*, 2013]. Cross sections A–A′ and B–B′ were drafted by hand at 1:24,000 scale [*Long*, 2014] and are presented here at ~1:100,000. Apparent dips of supporting attitude measurements were projected onto the cross sections, and areas of similar apparent dip were divided into dip domains. Boundaries between adjacent dip domains were treated as kink surfaces [e.g., *Suppe*, 1983], with their orientations determined by bisecting the interlimb angle. Estimates of fault dip angles at the modern erosion surface (Table 1) were calculated using three-point problems and bracketing constraints obtained from cross section geometry (supporting data in the supporting information). Combining dip domains and fault dip angles allowed calculation of stratigraphic cutoff angles of set 1 faults at the modern erosion surface (Table 1). In addition, lithologic logs and apparent dip data for 10 wells in the Grant Canyon and Bacon Flat oil fields (Figure 2) are projected onto A–A′ (supporting data in the supporting information).

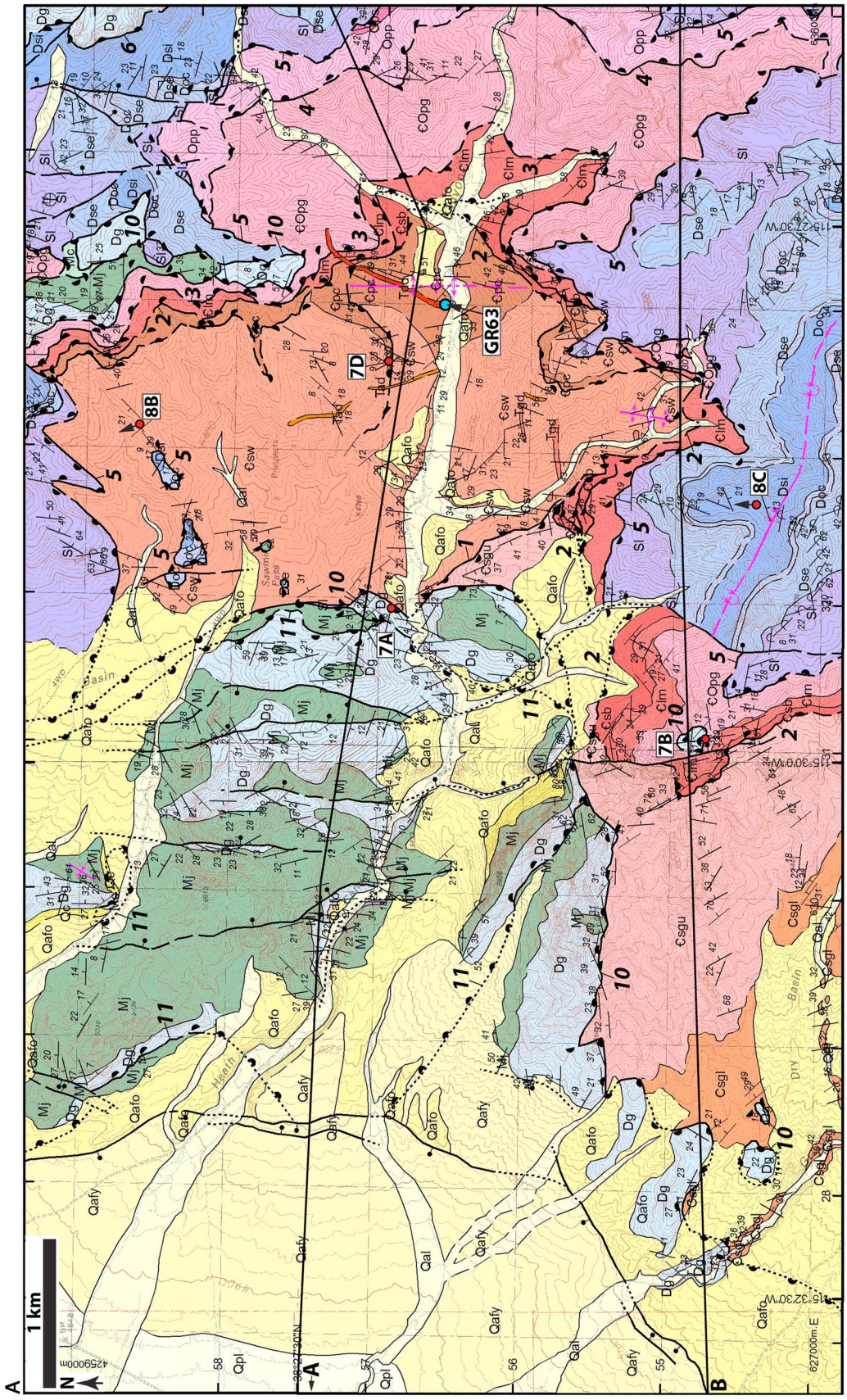

Figure 4. Geologic map of central Grant Range, centered on Heath Canyon [modified from *Long*, 2014], divided into (a) western half and (b) eastern half. Location of $^{40}Ar/^{39}Ar$ sample GR63 shown, along with locations of field photographs of Figure 7, locations and view directions of field photographs of Figure 8, and lines of cross sections. Set 1 detachment faults are numbered. Guide to map units and symbology shown in Figure 3.

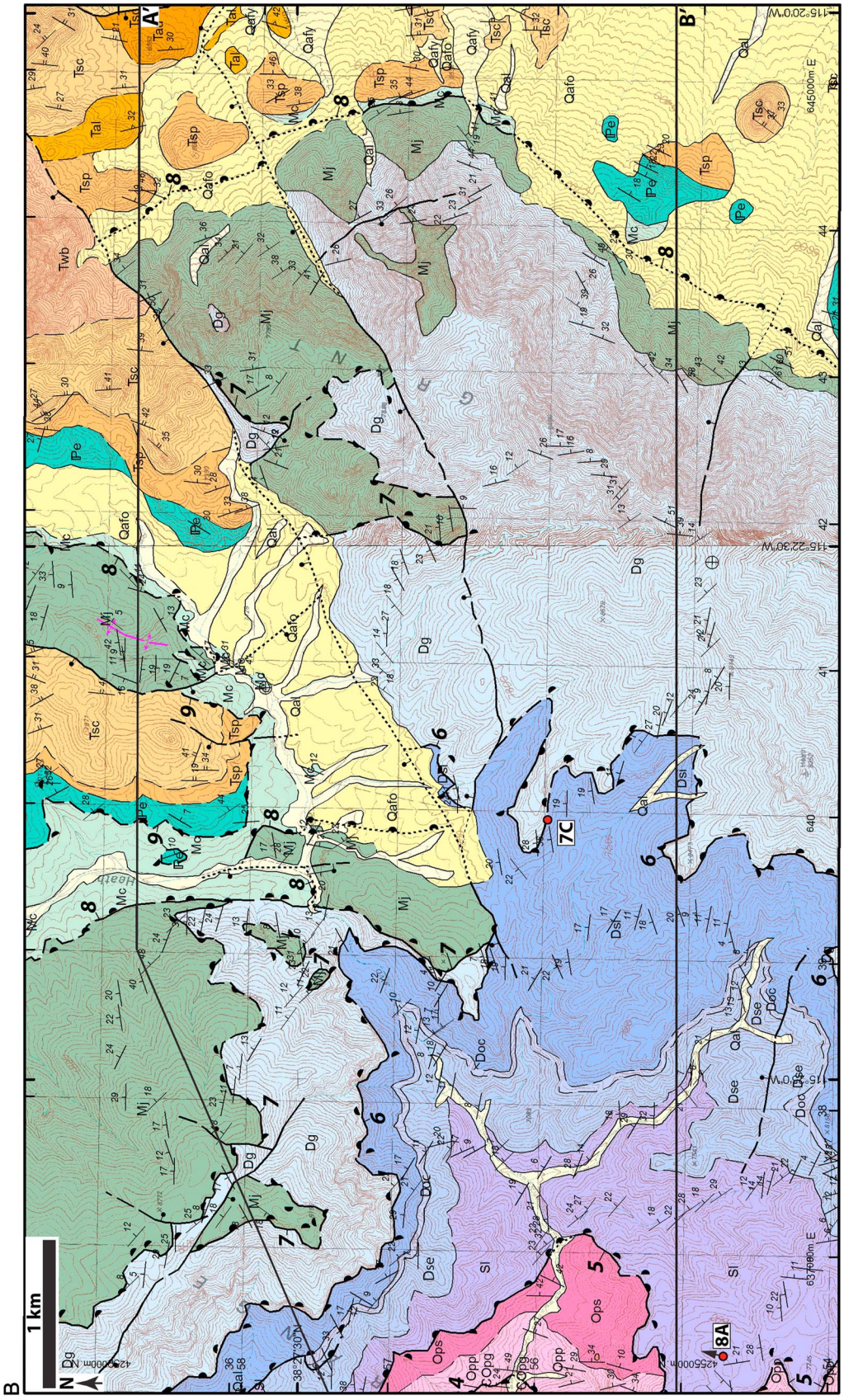

Figure 4. (continued).

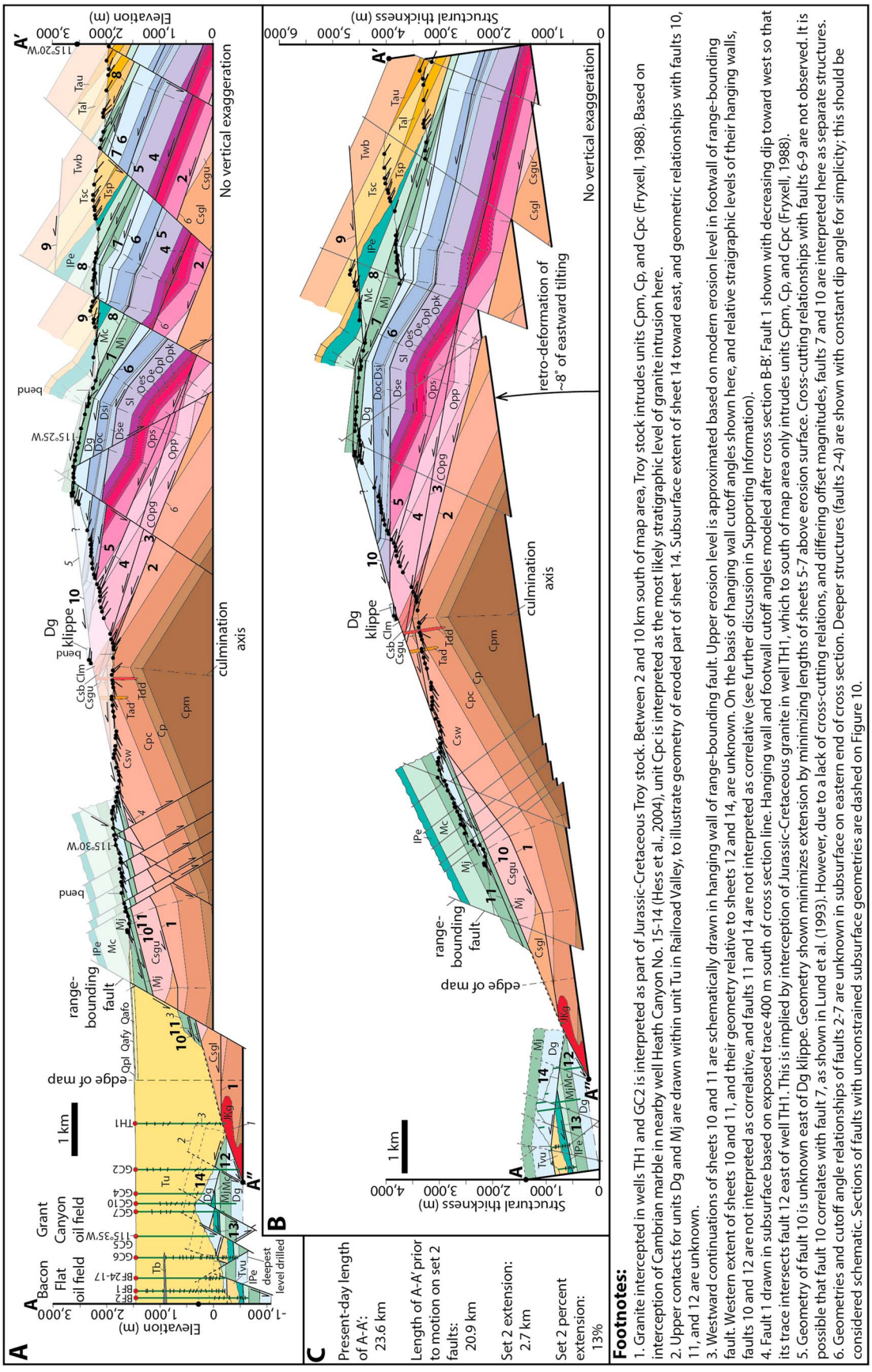

Footnotes:

1. Granite intercepted in wells TH1 and GC2 is interpreted as part of Jurassic-Cretaceous Troy stock. Between 2 and 10 km south of map area, Troy stock intrudes units Cpm, Cp, and Cpc (Fryxell, 1988). Based on interception of Cambrian marble in nearby well Heath Canyon No. 15-14 (Hess et al., 2004), unit Cpc is interpreted as the most likely stratigraphic level of granite intrusion here.
2. Upper contacts for units Dg and Mj are drawn within unit Tu in Railroad Valley, to illustrate geometry of eroded part of sheet 14. Subsurface extent of sheet 14 toward east, and geometric relationships with faults 10, 11, and 12 are unknown.
3. Westward continuations of sheets 10 and 11 are schematically drawn in hanging wall of range-bounding fault. Upper erosion level is approximated based on modern erosion level in footwall of range-bounding fault. Western extent of sheets 10 and 11, and their geometry relative to sheets 12 and 14, are unknown. On the basis of hanging wall cutoff angles shown here, and relative stratigraphic levels of their hanging walls, faults 10 and 12 are not interpreted as correlative, and faults 11 and 14 are not interpreted as correlative (see further discussion in Supporting Information).
4. Fault 1 drawn in subsurface based on exposed trace 400 m south of cross section line. Hanging wall and footwall cutoff angles modeled after cross section B-B'. Fault 1 shown with decreasing dip toward west so that its trace intersects fault 12 east of well TH1. This is implied by interception of Jurassic-Cretaceous granite in well TH1, which to south of map area only intrudes units Cpm, Cp, and Cpc (Fryxell, 1988).
5. Geometry of fault 10 is unknown east of Dg klippe. Geometry shown minimizes extension by minimizing lengths of sheets 5-7 above erosion surface. Cross-cutting relationships with faults 6-9 are not observed. It is possible that fault 10 correlates with fault 7, as shown in Lund et al. (1993). However, due to a lack of cross-cutting relations, and differing offset magnitudes, faults 7 and 10 are interpreted here as separate structures.
6. Geometries and cutoff angle relationships of faults 2-7 are unknown in subsurface on eastern end of cross section. Deeper structures (faults 2-4) are shown with constant dip angle for simplicity; this should be considered schematic. Sections of faults with unconstrained subsurface geometries are dashed on Figure 10.

Figure 5. (a) Cross section A–A'; line of section shown in Figures 2 and 4, locations of oil wells shown in Figure 2, map units shown in Figure 3. Set 1 faults labeled in bold numbers. Footnotes with justifications for individual drafting decisions labeled in italics. Translucent areas above modern erosion surface represent eroded rock. (b) Partially restored version of A–A', with motion and tilting accommodated by set 2 normal faults retrodeformed (see supporting information for methodology and supporting data). Quaternary map units are omitted. (c) Supporting data for estimation of extension accommodated by set 2 normal faults.

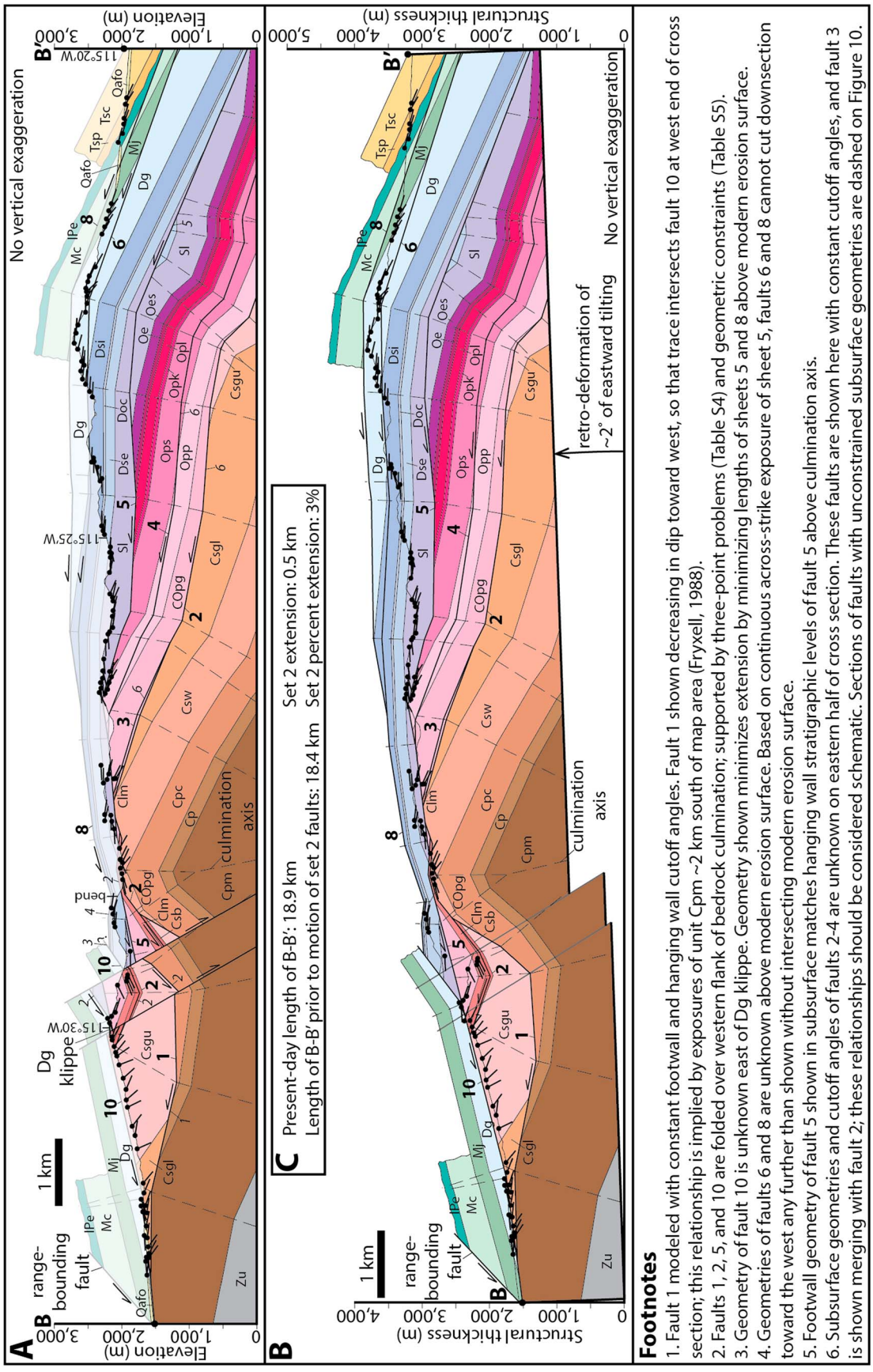

Footnotes

1. Fault 1 modeled with constant footwall and hanging wall cutoff angles. Fault 1 shown decreasing in dip toward west, so that trace intersects fault 10 at west end of cross section; this relationship is implied by exposures of unit Cpm ~2 km south of map area (Fryxell, 1988).
2. Faults 1, 2, 5, and 10 are folded over western flank of bedrock culmination; supported by three-point problems (Table S4) and geometric constraints (Table S5).
3. Geometry of fault 10 is unknown east of Dg klippe. Geometry shown minimizes extension by minimizing lengths of sheets 5 and 8 above modern erosion surface.
4. Geometries of faults 6 and 8 are unknown above modern erosion surface. Based on continuous across-strike exposure of sheet 5, faults 6 and 8 cannot cut downsection toward the west any further than shown without intersecting modern erosion surface.
5. Footwall geometry of fault 5 shown in subsurface matches hanging wall stratigraphic levels of fault 5 above culmination axis.
6. Subsurface geometries and cutoff angles of faults 2-4 are unknown on eastern half of cross section. These faults are shown here with constant cutoff angles, and fault 3 is shown merging with fault 2; these relationships should be considered schematic. Sections of faults with unconstrained subsurface geometries are dashed on Figure 10.

Figure 6. (a) Cross section B–B'; line of section shown in Figures 2 and 4, map units shown in Figure 3 (unit Zu represents undifferentiated Neoproterozoic sedimentary rocks, which presumably underlie unit Cpm [e.g., *Stewart*, 1980] and are not shown in Figure 3). Set 1 faults labeled in bold numbers. Footnotes with justifications for individual drafting decisions labeled in italics. Translucent areas above modern erosion surface represent eroded rock. (b) Partially restored version of B–B', with motion and tilting accommodated by set 2 normal faults retrodeformed (see supporting information for methodology and supporting data). Quaternary map units are omitted. (c) Supporting data for estimation of extension accommodated by set 2 faults.

Table 1. Geometric Constraints, Offset Estimates, and Crosscutting Relationships for Set 1 Faults[a]

Cross section A–A′

Fault Number	Dip Angle at Modern Erosion Surface or Defined by Well Data	Stratigraphic Cutoff Angle at Modern Erosion Surface or Defined by Well Data	Offset (m)	Crosscutting Relationships
14	14°E[b] (between wells TH1 and GC6) 0°W[b] (west of well GC6)	−14° (footwall; east of GC6), 0° (footwall; west of GC6) 0° (hanging wall)	2,600 minimum	branches off 12 (inferred) cuts 13 (required) cuts Tvu (observed)
13	2°W[b] (west of well GC10)	2°	1,600 minimum	
12	20°W[b] (west of well TH1)	20° (hanging wall; sheet 12), 34° (hanging wall; sheet 14) 28°(footwall; autochthon), 40° (footwall; sheet 1)	2,800 minimum	
11	14°W[b]	−3°	4,000 minimum	cuts 10 (observed)
10	8°W[b] minimum (east of Dg klippe) 12°W[b] (Dg klippe to main trace) 14°W[b] (west of main trace)	−3° (hanging wall; main exposure) 13° (hanging wall; Dg klippe) −9° (footwall; autochthon) 44° (footwall; sheets 2, 3) 40° minimum (footwall; sheet 4) 43° minimum (footwall; sheet 5) 18° minimum (footwall; sheets 6, 7)	7,000 minimum	cuts 1, 5 (observed) cuts 2, 3, 4 (required) cuts 6 (inferred)
9	3°E[c]	27° (Paleozoic rocks), 30° (Tertiary rocks)	700	merges with 8 (inferred) cuts Tsp, Tsc (observed) cuts Twb (required)
8	25°E[b]	5° (Paleozoic rocks), 8° (Tertiary rocks)	4,100	cuts 7 (observed) cuts Tsp (required)
7	13°E[c]	−2°	4,800	cuts 6 (observed)
6	7°E[c]	3°	4,300	
5	**8°E[c]** **11°W[c] (N of cross-section line)**	3°	2,500 minimum	cuts 2, 3, 4 (observed)
4	23°E[c]	9°	600 minimum	
3	17°E[c]	15°	50 minimum	cuts 2 (observed) cut by Tdd (observed)
2	21°E[c]	12°	14,950	cuts 1 (observed) cut by Tdd (observed)
1	**0–30°W range[b]**	22° (hanging wall; after B–B′) 8° (footwall)[b]	5,400	

Cross Section B–B′

Fault Number	Dip Angle at Modern Erosion Surface	Cutoff Angle at Modern Erosion Surface	Offset (m)	Crosscutting Relationships
10	**33°W[b] minimum (east of Dg klippe)** **13°W[b] (Dg klippe to eastern trace)** **5°W[b] (between western three traces)**	−7° to 2° (hanging wall) 16° (footwall; autochthon) 26–48° (footwall; sheet 1) 35° minimum (footwall; sheet 2) 32° minimum (footwall; sheet 5)	4,600 minimum	cuts 1 (observed) cuts 2, 5 (required)
8	19°E[b]	6° (Tertiary and Paleozoic rocks)	3,100	cuts 6 (inferred)
6	0–2°W[b] (between traces)	2–7°	1,300	
5	**16°E[c] (east of easternmost trace)** **5–7°W[b] (between traces)** **13°W[b] (west of western trace)**	10° to −16° range (hanging wall)[b] 10° (footwall, east of easternmost trace)[b]	8,850	cuts 2, 3, 4 (observed) cuts Tgd (observed)
4	23°E[c] (east of trace) 1°E[b] (west of trace)	3°	50 minimum	
3	17°E[c] (east of eastern trace) 3°E[b] (east side culmination window)	9° (east of culmination axis)	50 minimum	merges with 2 (inferred)
2	**17°E[c] (east of eastern trace)** **5°E–5°W[b] (at culmination window)** **35°W–21°E[b] (between western traces)**	10° (east of culmination axis) 0–13° (west of culmination axis)	13,300	cuts 1 (observed) cut by Tgd (observed)
1	**13°E–59°W range[b]**	22° minimum (hanging wall)[b] 10° minimum (footwall)[b]	5,150	

[a]Positive cutoff angles indicate fault cuts downsection toward west, and negative cutoff angles indicate fault cuts upsection toward west. Offset estimates for faults 10–14 are minimum structural overlap of drafted areas in Figures 5 and 6. Cells in bold highlight data that support folding across axial zone of culmination.
[b]Constrained by cross-section geometry; supporting data in Table S5.
[c]Constrained by a three-point problem; supporting data in Table S4.

Thicknesses of rock units (Figure 3) were measured from the cross sections. For rock units that did not have complete sections exposed in the map area, thicknesses reported in published studies in the Grant Range [*Moores et al*., 1968; *Cebull*, 1970; *Hyde and Huttrer*, 1970; *Fryxell*, 1988; *Camilleri*, 2013] were utilized, and in the case where complete thicknesses were not exposed anywhere in the Grant Range, minimum tectonic thicknesses estimated from the cross sections were used (supporting data in the supporting information).

On the cross sections, offset linear features and angular relationships across faults were drafted so that they are internally consistent and retrodeformable. Therefore, the cross sections represent viable geometric solutions [*Elliott*, 1983]. However, they do not represent unique solutions. In particular, because the study area has experienced polyphase extension, one of the largest uncertainties is how to model fault geometries at great depths below the modern erosion surface, especially for the gently dipping set 1 faults. In the eastern part of each cross section, the subsurface geometry of the vertically stacked series of set 1 faults is the largest uncertainty in drafting and retrodeformation, and we emphasize that other viable solutions are possible.

Figures 5b and 6b show versions of A–A′ and B–B′ that have been retrodeformed for offset and tilting accommodated by set 2 faults. Offset on individual faults was retrodeformed by restoring the locations of matching structures and stratigraphic cutoffs. The magnitude of tilting was estimated on each cross section by calculating the cumulative offset magnitude of all set 2 faults and then treating the cross section as a coherent block that pivoted from its western end by the cumulative offset magnitude (description of methods in the supporting information). This simple restoration assumes that tilt magnitude was homogeneous across each cross section and that tilting accommodated by faults to the east and west of the cross section is negligible and should therefore be considered approximate. For A–A′, ~8° of eastward tilting was estimated (Figure 5b), and for B–B′, on which the cumulative offset on set 2 faults in Railroad Valley was projected from A–A′, ~2° of eastward tilting was estimated (Figure 6b). These gentle tilt magnitudes are corroborated by the characteristic ~5–10°E apparent dip of Neogene valley fill sediment on the majority of oil wells projected onto A–A′ (Figure 5a). Several wells also exhibit shallowing of dips at progressively higher stratigraphic levels within the valley fill section, which is characteristic of synextensional infilling in half-grabens [e.g., *Leeder and Gawthorpe*, 1987].

Comparison of present-day and pre-set 2 lengths indicates 2.7 km of extension (13%) on A–A′ and 0.5 km (3%) on B–B′. Since A–A′ spans the Grant Range and part of Railroad Valley, this estimate is considered more representative. The pre-set 2 geometry (Figures 5b and 6b) is interpreted as a best approximation for the geometry after motion on set 1 detachment faults.

5. Set 1 Brittle Detachment Fault System

Set 1 faults are grouped genetically by their common low dip angle and low cutoff angle geometry, and by field relations indicating progressive emplacement within an integrated fault system. Set 1 faults are interpreted as normal because, in the majority of cases, they omit stratigraphic section, and some omit metamorphic isograds [*Lund et al*., 1993; *Camilleri*, 2013]. Although no independent estimates of kinematics on individual faults were observed, all set 1 faults are interpreted to be top-to-west [*Camilleri*, 1992, 2013; *Lund et al*., 1993], because matching stratigraphic cutoffs across individual faults are consistently offset toward the west in cross section (Figures 5 and 6), and in the majority of cases, set 1 faults cut stratigraphically downsection toward the west.

Most set 1 faults, particularly those developed in carbonate rocks, exhibit discrete, meter-scale zones of brecciation and calcite veining (Figure 7), indicating brittle conditions during extension. The set 1 faults that deform greenschist facies Cambrian and Ordovician rocks also exhibit breccia zones (Figure 7d), indicating that the Late Cretaceous peak thermal regime that produced this shallow-crustal metamorphism [*Fryxell*, 1988; *Camilleri*, 2013] had relaxed by the time extension initiated. In addition, several set 1 faults contain evidence for synemplacement or postemplacement fluid flow, including local alteration to lithologies such as jasperoid (Figure 8b).

5.1. A Note on Previous Work

Previous mapping-based studies in the Grant Range have yielded significant advances in understanding the geometry and style of set 1 extension, upon which this study builds. *Moores et al*. [1968], a pioneering

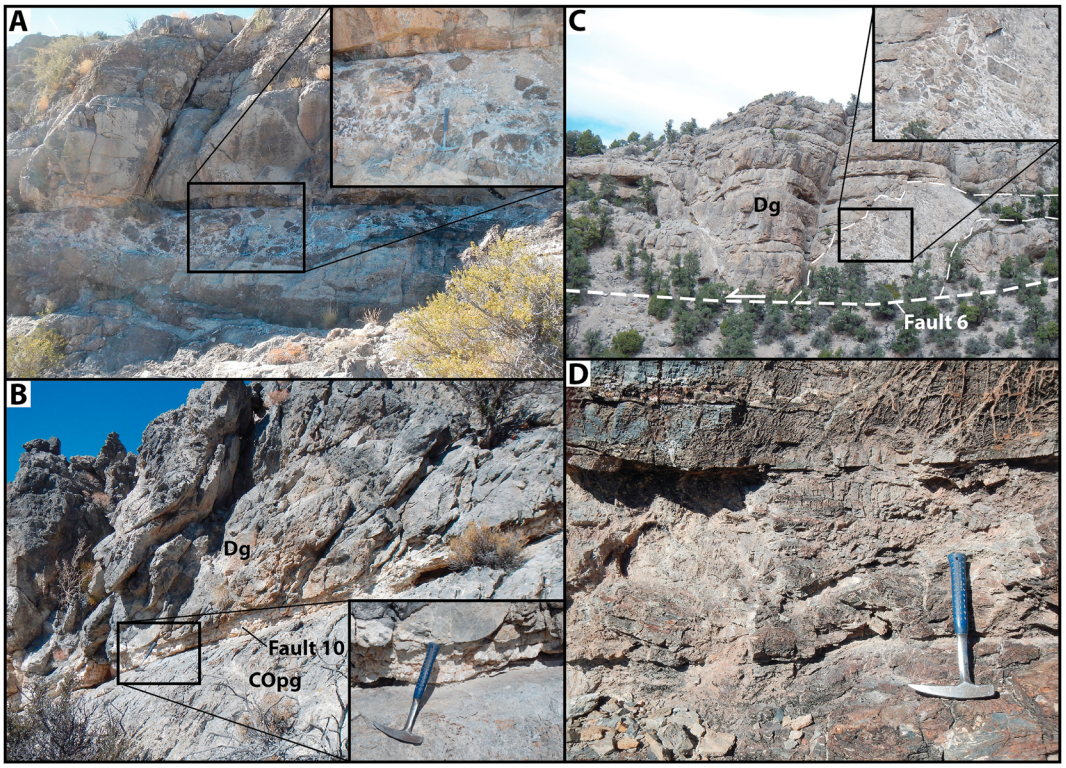

Figure 7. Field photographs showing characteristic deformation textures of set 1 fault zones; locations shown in Figure 4, unit abbreviations shown in Figure 3. (a) Approximately 1 m thick, intraformational, bedding-subparallel breccia zone within Dg limestone, ~5 m structural distance above fault 10 in Heath Canyon. (b) Approximately 30 cm thick calcite vein developed along fault 10, between brecciated Dg limestone in hanging wall and brecciated COpg limestone in footwall. (c) Breccia zone up to ~10 m thick, containing centimeter- to meter-scale breccia blocks of Dg limestone in calcite matrix, developed along and ~5–10 m structural distance above fault 6. Dg cliffs are up to ~20 m tall. (d) Approximately 30 cm thick, intraformational, bedding-subparallel breccia zone within Cpc limestone, ~5 m structural distance above an unnamed fault in Heath Canyon that places Cpc over Csw, which is the structurally lowest set 1 fault in the map area.

study in the White Pine Range and northern Grant Range, mapped several low-angle, younger-over-older faults and was the first to interpret them as related to Tertiary extension. Following this, the work of *Lund et al*. [1993], which is supported by 1:50,000 scale, range-wide mapping of the central and northern Grant Range [*Lund et al*., 1987, 1988], was the first to assert that extension was accommodated by a stacked set of west-vergent detachment faults that formed at low angles to bedding and that extension was accompanied by arching. In addition, *Camilleri* [1992, 2013], based on mapping in the west-central part of the range, presented field relations describing the bottom-to-top growth of the detachment system, and progressive rotation of older detachment faults. Finally, in the southern Grant Range, *Fryxell* [1988] mapped two sets of low-dip-angle normal faults, an older, ESE-vergent set, and a younger, WSW-vergent set.

The following sections expand on the interpretations of these early studies by presenting quantitative descriptions of field relations, fault geometries, and extension magnitude, and a model for the kinematic development of the set 1 fault system. We then explore implications for primary low-angle normal fault slip, the magnitude of synextensional isostatic flexure, and the style of extension within the upper plates of core complex-type fault systems.

5.2. Set 1 Fault Divisions, Geometries, and Field Relations

Eleven distinct set 1 faults can be mapped and correlated in the Grant Range (Figures 4–6), and three additional faults are defined by well data in Railroad Valley (Figure 5), which divides the map area into 14 structural sheets, which are listed in Figure 9 by the basal fault that carried them. The structurally lowest sheet is labeled as an autochthon in Figure 9 and is interpreted to have been spatially fixed during the westward translation of sheets 1–14. In cross section, sheets 1–14 range in vertical thickness from 50 to 1000 m but are typically 200–500 m

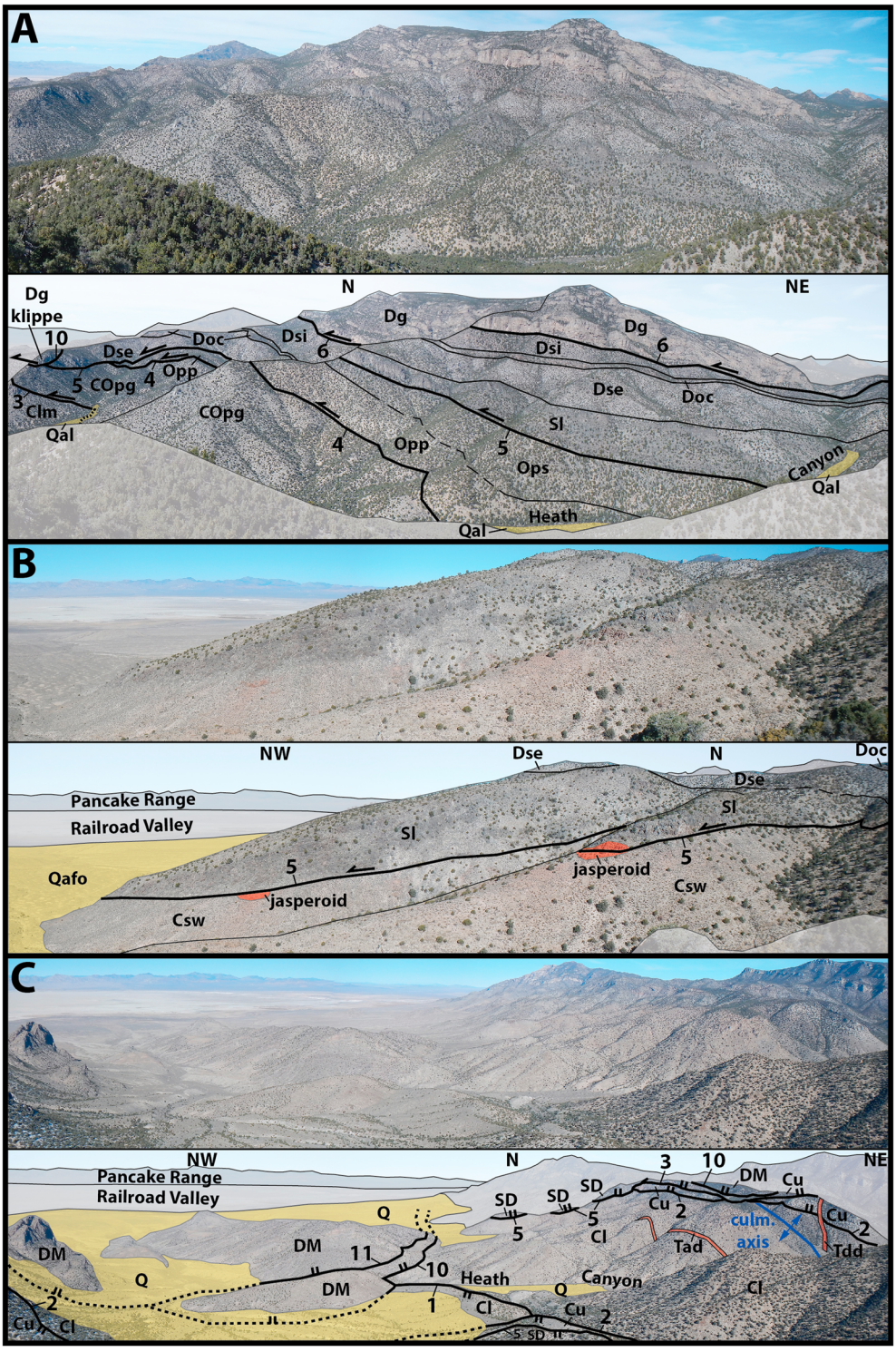

Figure 8. Original and annotated field photographs; locations and view directions shown in Figure 4, unit abbreviations shown in Figure 3. (a) View of north side of Heath Canyon, east of culmination axis, showing gently east dipping faults 3–6 omitting strata within gently east dipping Cambrian through Devonian rock units. Crosscutting relationships between faults 4, 5, and 10 are annotated. (b) View of fault 5, west of culmination axis, dipping gently west and placing Silurian rocks over Cambrian rocks. (c) View of north side of Heath Canyon, showing fault geometries west of culmination axis. Crosscutting relationships between faults 1, 2, 3, 5, 10, and 11, and between fault 2 and ~29 Ma dacite dike (Tdd), are annotated. Simplified rock units: Cl = units Csw and Csgu; Cu = units Csb, Clm, and COpg; SD = Silurian-Devonian, undifferentiated; DM = Devonian-Mississippian, undifferentiated; Q = Quaternary, undifferentiated.

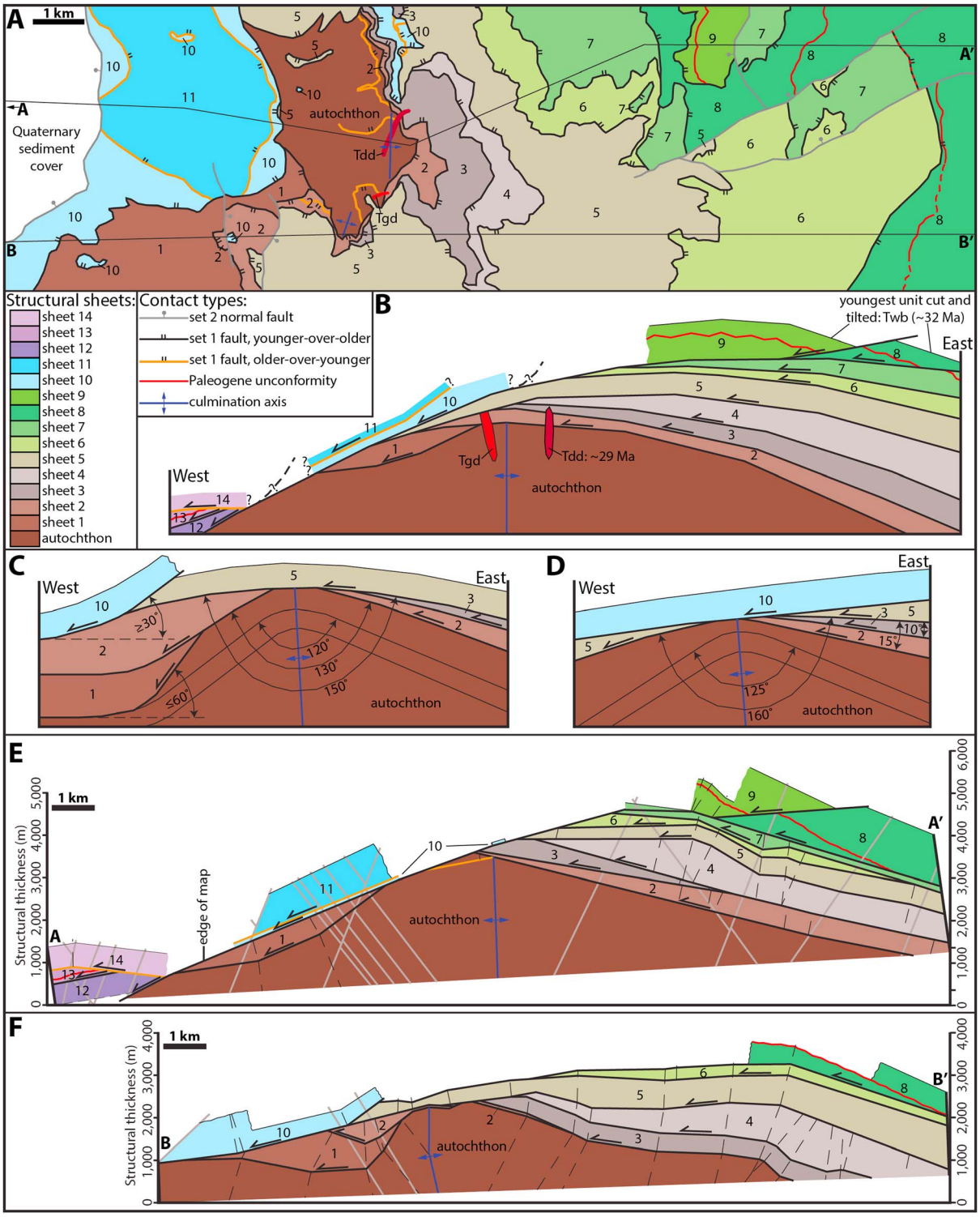

Figure 9. Diagrams summarizing field relationships. (a) Simplified version of Figure 4, divided into structural sheets that are colored and labeled by the set 1 fault at their base. Segments of faults that omit strata shown in black, and segments that duplicate strata shown in orange (many older-over-younger relationships occur along second-order faults that were not individually numbered). Crosscutting relationships between faults, granite dike (Tgd), ~29 Ma dacite dike (Tdd), and Paleogene unconformity are visible. (b) Schematic cross section summarizing crosscutting relationships between faults, dikes, and Paleogene unconformity. (c, d) Schematic diagrams summarizing folding and incision relationships across culmination axis on south (Figure 9c) and north (Figure 9d) sides of Heath Canyon. Increasing interlimb angles between the limbs of the autochthon and faults 2 and 5 and incision through sheets 2 and 3 by fault 5 (Figure 9c) and sheets 2, 3, and 5 by fault 10 (Figure 9d) indicate synextensional growth of culmination. (e, f) Simplified versions of Figures 5b and 6b, divided into the same structural sheets as diagrams in Figures 9a and 9b.

thick. Some sheets can be continuously traced across strike for map distances up to 10 km (e.g., sheets 5 and 6) and in excess of 15 km in cross section (e.g., sheet 5).

Crosscutting relationships, summarized on Table 1 and Figure 9, demonstrate that structurally higher faults cut structurally lower faults, indicating that the system developed from bottom to top. Faults 1–9 represent a coherently exposed series in the eastern and central Grant Range that are labeled in the order in which they were emplaced (Figure 9). Faults 10 and 11 are exposed in the western Grant Range; fault 10 is younger than faults 1–5, does not display crosscutting relationships with faults 6–9, and is cut by fault 11. In Railroad Valley, faults 12–14 can be placed in relative order of emplacement, but crosscutting relationships between faults 10–11 and 12–14 are not observed. Detailed descriptions of the geometries and field relationships of faults 1–14 are included in the supporting information and are summarized in Table 1. Below, groups of set 1 faults that exhibit important field relationships are discussed.

5.2.1. Imbricate Stack in Central and Eastern Grant Range

The eastern two thirds of the Grant Range is defined by a stacked, overlapping series of ~0–25°E dipping sheets carried by faults 2 through 9, with each fault cutting downsection toward the west at typical cutoff angles of 5–15°. Faults 2–9 exhibit crosscutting relationships, indicating that they were emplaced from structurally lowest to highest (Table 1 and Figure 9). In addition, faults 2 and 3 are cut by a ~29 Ma (sample GR63; Figure 4), NE trending dacite dike on the north side of Heath Canyon, and fault 2 is cut by an undated, E trending granite dike on the south side of Heath Canyon, and this granite dike is cut by fault 5 [*Camilleri*, 2013] (Figures 4 and 9). On the east end of the range, faults 8 and 9 cut rocks above the Paleogene unconformity, with fault 9 cutting Paleogene rocks as young as ~32 Ma (Figures 4, 5, and 9).

The Paleogene unconformity is exposed in the eastern part of the range, at erosion levels within units lPe and Mc, and the uniform ~30°E dip of rocks above and below defines minimal angular discordance (Figures 5 and 6). Conodont alteration indices of 1–1.5 from Pennsylvanian and Mississippian rocks in this region indicate a maximum burial temperature range of ~50–80°C [*Harris et al*., 1980; *Konighshof*, 2003; *Crafford*, 2007], which indicates that the erosion surface at the time of set 1 extension cannot have been more than ~2–3 km above the Paleogene unconformity, assuming a geothermal gradient of ~25–30°C/km. Therefore, faults 8 and 9, which cut Paleogene rocks above the unconformity, record low cutoff angle detachment faulting at very shallow depths. At its exposure, fault 9 cuts through at least ~500 m of Paleogene rocks (Figures 4 and 5), and the fault is not observed within a ~1.5 km thick section of Paleogene rocks exposed to the east of its trace. Therefore, fault 9 must cut upsection through at least 1.5 km of Paleogene rocks above the modern erosion surface (Figure 5) and thus records faulting at depths as shallow as ~0.5–1.5 km below the paleo-erosion surface at the time of set 1 faulting.

5.2.2. Structural Culmination in Western Grant Range

The apex of a N trending structural culmination is observed in the western Grant Range and is represented in the autochthon by an anticline with limb dips of 25–35° (Figures 4–6), defining interlimb angles of 120–125° (Figures 9c and 9d), and by a pronounced change in the dip direction of set 1 faults. West of the culmination axis, faults 1, 2, 5, and 10–14 dip ~0–30°W, whereas east of the axis, faults 2 through 9 in the imbricate stack dip ~0–25°E (Figures 5 and 6). In addition, the traces of faults 2 and 5 exhibit folding across the culmination axis, which is apparent in their map patterns (Figures 4 and 9) and in cross section. On B–B′, over an across-strike distance of 3 km, the dip of fault 2 changes from 17°E at its easternmost trace to 5°E and 5°W as it crosses the axial zone to a minimum subsurface dip of 35°W toward the west (Table 1 and Figure 6), defining an interlimb angle of ~130° (Figure 9c). On B–B′, over an across-strike distance of 6 km, the dip of fault 5 changes from 16°E at its easternmost trace to 5–7°W between the four traces that intersect the cross-section line to 13°W at its westernmost trace, defining an interlimb angle of ~150° (Table 1 and Figure 9c). On the north side of Heath Canyon, over an across-strike distance of 4 km, fault 5 changes from a dip of 8°E east of the culmination axis to subhorizontal in proximity to the axis to 11°W west of the axis, defining an interlimb angle of ~160° (Table 1 and Figure 9d).

In the western limb of the culmination, faults 1 and 10 shallow in dip angle toward the west on B–B′, providing further evidence for folding. Over an across-strike distance of 4 km, the dip of fault 10 shallows from a minimum of 33°W above the modern erosion surface east of a klippe of unit Dg to 13°W between the klippe and the easternmost of three traces exposed on the western flank of the range to 5°W between these three traces (Figures 6 and 9c). Also, exposures of unit Cpm south of the map area [*Fryxell*, 1988]

indicate that the trace of fault 1 is shallowly buried at the western end of B–B′, which implies a westward shallowing of dip angle (Table S5). On B–B′, fault 1 is shown flattening from a dip of 60°W to subhorizontal over an across-strike distance of 2 km; however, because this geometry is based on the assumption of constant cutoff angles across strike, this magnitude of folding is interpreted as a maximum (Figure 9c).

In the imbricate stack in the eastern limb, structurally lower faults progressively increase in structural elevation relative to younger, structurally higher faults (Figures 5, 6, and 9), resulting in increased stratigraphic omission, and therefore increased vertical thinning, as the culmination axis is approached. This is best demonstrated by the relationship between sheets 2–4 and sheet 5 on cross section B–B′, where multiple traces of fault 5 are exposed across strike (Figure 6). Field relations also demonstrate progressive incision of older sheets by younger faults over the culmination axis. On the south side of Heath Canyon, sheet 2 is observed underneath sheet 5 to the east and west of the culmination axis, but in the axial zone, fault 5 incises through sheet 2 for an across-strike distance of 300 m, placing sheet 5 directly over the autochthon (Figures 4 and 9c). Similarly, on the northern edge of the map area, sheet 5 is observed on the east and west sides of the culmination axis, but in the axial zone, fault 10 has incised through sheet 5, placing sheet 10 directly over sheet 3 (Figures 4 and 9d).

5.2.3. Faults in Western Grant Range and Subsurface of Railroad Valley

In the western Grant Range, fault 10 places Devonian and Mississippian rocks over Cambrian rocks in the autochthon (Figures 4 and 9a), corresponding to omission of 5200–5400 m of stratigraphy. The main trace of fault 10 is correlated with faults bounding several klippen of unit Dg in the southwest corner of the map area, and a fault bounding the base of an exposure of Devonian and Mississippian rocks at the culmination axis on the north side of Heath Canyon (Figures 4 and 9a). East of the culmination axis, the geometry of fault 10 is unconstrained. Fault 10 cuts fault 5 and carries stratigraphically higher rocks than fault 6, which implies that fault 10 is younger. However, in the absence of crosscutting relationships, its relative order of emplacement with faults 7–9 is unknown (Figure 5, footnote 5). In the western Grant Range, fault 11 duplicates 200–400 m of Devonian and Mississippian rocks over the top of sheet 10 (Figures 4 and 5), defining an apparent thrust relationship. Two segments of fault 11 were originally mapped as thrust faults by *Lund et al.* [1987, 1988]. Fault 11 cuts fault 10 on the south side of Heath Canyon (Figures 4 and 9a); however, its relative order of emplacement with faults 7–9 is unknown.

In the subsurface of Railroad Valley, well data define three additional set 1 faults (Figure 5). Fault 12 is the name given to the structure that places Devonian rocks over Jurassic-Cretaceous granite in well GC2 (Figure 5). Stratigraphic omission across fault 12 at well GC2 is estimated at 5400–6200 m. Fault 12 is shown at its minimum possible dip of 20°W, as defined by intersection depths of granite in wells TH1 and GC2. The geometry of fault 12 east of well TH1 is unconstrained (Figure 5, footnote 3); it is possible that faults 12 and 10 share a similar footwall level, as shown on A–A′, which would define a master detachment level for the set 1 fault system in the western limb of the culmination. Devonian and Mississippian rocks carried by fault 12 are bound above by fault 13, a bedding-subparallel fault defined above a ~50–75 m thick section of unit Mc that is interpreted as structurally thinned. Fault 13 carries unit IPe in its hanging wall, which is unconformably overlain by Paleogene volcanic rocks. Subhorizontal to gently east dipping apparent dips in rocks above and below the Paleogene unconformity (Figure 5) indicate minimal angular discordance, similar to observations in the eastern Grant Range.

Above sheets 12 and 13, unit Dg is intercepted in multiple wells, defining an older-over-younger structure that is here named fault 14. This older-over-younger relationship has previously been interpreted as a Mesozoic thrust fault [*Hulen et al.*, 1994; *McCutcheon and Zogg*, 1994] or a Tertiary landslide block that slid westward from the Grant Range [*French*, 1993; *Johnson*, 1993]. In this study, we correlate fault 14 with the set 1 fault system, and a kinematic model is presented below (section 6.1) that places fault 14 in this context. On A–A′, fault 14 is shown with an apparent thrust geometry, ramping upsection toward the west through 900 m of Mississippian, Pennsylvanian, and Paleogene rocks in its footwall. No crosscutting relationships between faults 12 and 14 are exposed, but fault 14 is inferred to branch westward off of fault 12 (additional discussion in the supporting information).

5.3. Restoration of Set 1 Extension

To illustrate the pre-extensional geometry of the study area, retrodeformation of offset on set 1 faults was performed (Figure 10). For smaller-offset faults (e.g., faults 3, 4, and 9), offset was retrodeformed by restoring

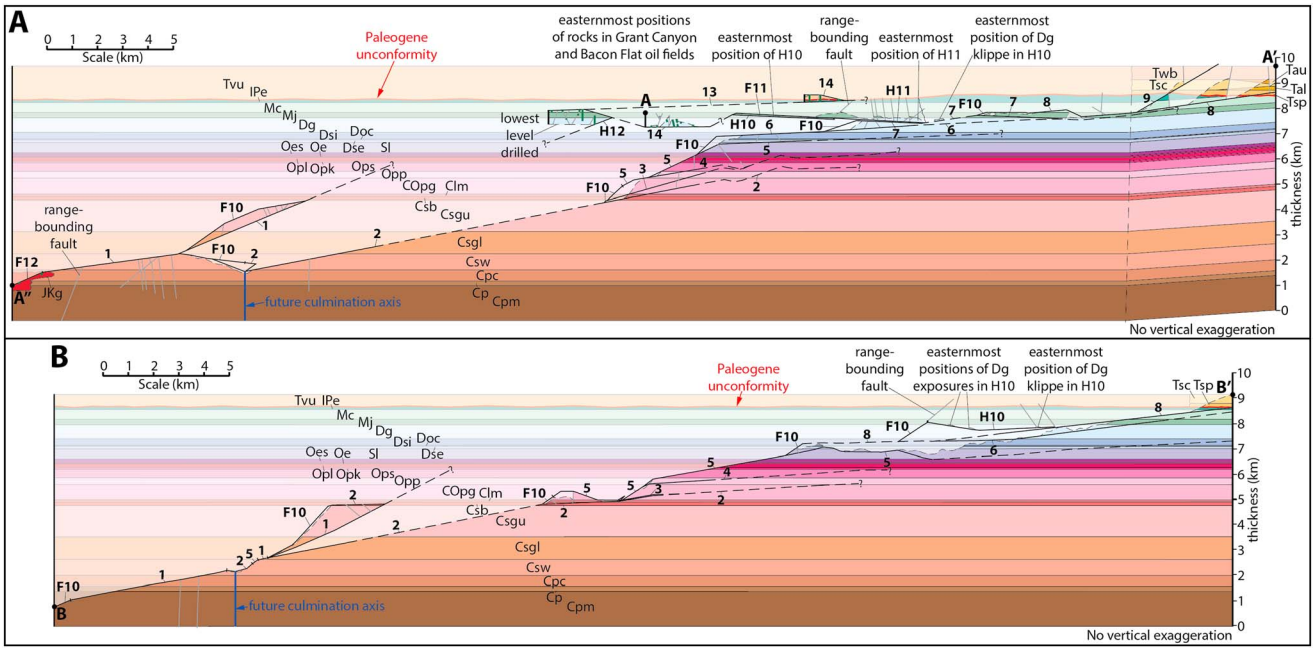

Figure 10. Cross sections (a) A–A′ and (b) B–B′, with offset along set 1 detachment faults restored and with Paleozoic and Paleogene rocks restored to horizontal (3° dip difference across Paleogene unconformity shown on east end of Figure 10a). Set 1 faults are labeled in bold numbers; for faults 10–12, "F" and "H" represent the restored positions of rocks in the footwall and hanging wall, respectively. Dashed portions of set 1 faults represent sections with unconstrained geometries. Gray lines represent restored positions of set 2 faults. Translucent areas represent rock that has either been eroded above the modern erosion surface (thin dashed line) or translated westward off of the study area during set 1 extension. The restored positions of sheets 10–14 are unknown; here they are shown at their easternmost permissible restored position.

the locations of matching stratigraphic cutoffs. For large-offset faults that did not have matching stratigraphic cutoffs on the drafted area of Figures 5 and 6 (e.g., faults 1 and 2), estimates of stratigraphic cutoff angles at the modern erosion surface (Tables 1, S4, and S5) were integrated with stratigraphic thicknesses (Table S1) to estimate offset; this required assumption of constant cutoff angles across strike for these faults. Also, since minimum thicknesses were used for several rock units (Table S1) and because drafting decisions were designed to minimize structural overlap where possible (e.g., Figure 5, footnote 5), offset estimates on many structures should be considered as minima (Table 1).

Polyphase extension makes determination of the precise initial geometry of the study area difficult, in particular determining pre-extensional dip magnitudes of Paleozoic rocks. However, several observations indicate that Paleozoic rocks must have been gently dipping prior to set 1 extension. In the eastern Grant Range and in Railroad Valley, the Paleogene unconformity records minimal (~0–3°) angular discordance with Paleozoic rocks (Figures 4–6). Set 1 extension had to have begun by the late Oligocene (~29 Ma), and there is no evidence for any earlier extension in the study area. Also, within the study area and along strike in the Grant Range, no differential tilting is observed within the late Eocene to Oligocene volcanic section or between these volcanic rocks and the underlying Paleocene-Eocene Sheep Pass Formation [*Moores et al.*, 1968; *Lund et al.*, 1993]. Therefore, Paleogene rocks, and the Paleozoic rocks that lay directly beneath them, must have been subhorizontal when set 1 extension began. In addition, the stratigraphic level of the Paleogene unconformity, both in the eastern Grant Range and in Railroad Valley (Figures 4–6), is within units Mc or IPe, indicating a maximum pre-extensional structural relief of 600 m (Figure 3). At a regional scale, across strike through White River Valley, the Grant Range, and Railroad Valley at the latitude of the study area, the Paleogene unconformity lies on map units ranging from Dg to IPe [*Long*, 2015], corresponding to a maximum pre-extensional structural relief of ~2.0 km [*Kellogg*, 1963; *Stewart*, 1980], and angular discordance across the unconformity is typically ~0–15° [*Long*, 2015].

The magnitude of folding of the set 1 fault system observed across the structural culmination, combined with field relations indicating progressive growth of the culmination during set 1 extension, also indicates that Paleozoic rocks had low pre-extensional dip angles. The axial zone of the culmination separates the

Table 2. Data Supporting Extension Estimates for Set 1 Fault System[a]

Cross Section A–A′ (Pin at Point A″)			Cross Section B–B′ (Pin at Point B)		
A″ to A′: pre-set 1 horizontal separation	50.3	km	B to B′: pre-set 1 horizontal separation	46.7	km
A″ to A′: post-set 1 horizontal separation	18.9	km	B to B′: post-set 1 horizontal separation	18.4	km
initial length (accounts for faults 1–9 only)	50.3	km	initial length (accounts for faults 1–8 only)	46.7	km
final length (accounts for faults 1–9 only)	81.7	km	final length (accounts for faults 1–8 only)	75.0	km
set 1 extension (faults 1–9 only)	**31.4**	**km**	**set 1 extension (faults 1–8 only)**	**28.3**	**km**
percent extension (faults 1–9 only)	**62**	**%**	**percent extension (faults 1–8 only)**	**61**	**%**
fault 10 minimum structural overlap[b]	7.0	km	fault 10 minimum structural overlap[d]	4.6	km
fault 11 minimum structural overlap	4.0	km	final length (faults 1–10)	79.6	km
fault 12 minimum structural overlap[c]	2.8	km	**minimum set 1 extension (faults 1–10)**	**32.9**	**km**
fault 13 minimum structural overlap	1.6	km	**minimum percent extension (faults 1–10)**	**70**	**%**
fault 14 minimum structural overlap	2.6	km			
faults 10–14, minimum structural overlap	18.0	km			
final length (faults 1–14)	99.7	km			
minimum set 1 extension (faults 1–14)	**49.4**	**km**			
minimum percent extension (faults 1–14)	**98**	**%**			

[a]Cells highlighted in bold represent data used to calculate cumulative extension and percent extension estimates.
[b]Measured to east edge of Dg klippe.
[c]Measured along projection of fault 12 to a point vertically below point A.
[d]Measured from point B to east edge of Dg klippe.

range into a domain of ~0–25°E dipping faults in the eastern limb and a domain of ~0–30°W dipping faults in the western limb (Figures 5 and 6). Within the axial zone, interlimb angles progressively increase in structurally higher, younger sheets, from ~120° in the autochthon to ~130° for fault 2 and ~150–160° for fault 5, and structurally lower sheets are progressively incised by younger, structurally higher faults (Figures 9c and 9d). In addition, increased stratigraphic omission accompanies gain in structural elevation in the imbricate stack as the axial zone is approached from the east (Figures 5 and 6). These observations collectively indicate progressive growth of the culmination during set 1 extension, and accompanying folding of set 1 faults. Retrodeformation of folding of set 1 faults results in restoration of Paleozoic rocks to gentle pre-extensional dip angles. Figure 10 shows solutions for the pre-set 1 geometry of A–A′ and B–B′, with Paleozoic rocks restored to horizontal and with horizontal lengths obtained from retrodeformation of offset on set 1 faults. This simple restoration assumes that all folding exhibited in the study area occurred during extension, and therefore, the geometries shown on Figure 10 should be interpreted as approximate.

To estimate the magnitude and percent extension accommodated by set 1 faults, restored lengths on Figure 10 are compared to deformed lengths on Figures 5b and 6b (Table 2). On cross section A–A′, point A″ is defined in the autochthon at the westernmost drafted extent of fault 12 and is treated as a stationary pinpoint (Figures 5b and 10a). Point A′ is defined in sheet 8 at the eastern border of the cross section. A″ and A′ are 50.3 km apart in Figure 10a and 18.9 km apart in Figure 5b, which accounts for motion on faults 1–9. This corresponds to 31.4 km of westward translation of point A′ relative to point A″, corresponding to 62% extension. The restored positions of rocks carried in the hanging walls of faults 10–14 are unknown; therefore, the cumulative minimum structural overlap on these faults (Table 2), as measured in Figures 5b and 6b, is interpreted as an absolute minimum for the amount of extension that they accommodated. This cumulative structural overlap is 18.0 km (Table 2), which yields a minimum of 49.4 km of extension, or 98%.

On cross section B–B′, point B is defined in the autochthon at the western end of the cross section and is treated as a stationary pin point, and point B′ is defined in sheet 8 at the eastern border (Figures 6b and 10b). Using similar techniques to cross section A–A′, faults 1–8 accommodated 28.3 km of extension, or 61%, and adding the minimum structural overlap on fault 10 yields a minimum of 32.9 km of extension, or 70% (Table 2). The minimum extension estimate for cross section A–A′ is considered more representative, as it includes set 1 faults in Railroad Valley. However, we emphasize that due to uncertainty in the restored positions of sheets 10–14 and due to incomplete exposure of the set 1 fault system as a result of synextensional and postextensional erosion, these extension estimates are cautiously interpreted as minima.

6. Discussion

6.1. Model for Kinematic Development of Set 1 Fault System

A kinematic model for set 1 extension in the Grant Range must account for the following first-order geometric observations:

1. Set 1 faults are discrete, top-down-to-west, low cutoff angle detachment faults, which comprise an integrated system that traversed the upper ~8–10 km of the crust and exhibit brittle fault zone textures at all exposed structural levels.
2. The study area contains an anticlinal culmination that folds set 1 faults. In the axial zone, interlimb angles progressively increase in younger, structurally higher faults, and older, structurally lower sheets are incised by younger faults. In the eastern limb, vertical thinning increases as the axial zone is approached. These observations define progressive synextensional growth of the culmination for the duration of set 1 extension.
3. The low structural relief and minimal angular discordance of the Paleogene unconformity, combined with the magnitude of synextensional folding that accompanied construction of the culmination, indicate that Paleozoic rocks had gentle dip angles prior to extension. Therefore, the typical 5–15° stratigraphic cutoff angles of set 1 faults approximate the primary dip angles at which they were active.
4. In the eastern limb of the culmination, set 1 faults define an imbricate stack and exhibit crosscutting relationships indicating a bottom-to-top progression of emplacement.
5. Older-over-younger structural relationships are exhibited by faults 11 and 14 in the western limb and by a series of second-order faults directly west of the culmination axis.

Several of these observations are explained by a kinematic model of detachment systems in metamorphic core complexes proposed by *Lister and Davis* [1989]. In the discussion below, the term "incision" refers to a detachment cutting downward into deeper structural levels, and "excision" refers to a detachment cutting upward into shallower structural levels, after *Lister and Davis* [1989]. In their model (Figure 11a), an early detachment surface becomes progressively folded as a result of denudation-induced isostatic rebound. With progressive folding, the updip section of the detachment is rotated to a point at which it becomes mechanically easier to break a new, structurally higher detachment, which splays upward off of the original detachment surface at its structural apex. This represents excision, because it cuts through progressively higher structural levels of the upper plate. With continued extension and isostatic rebound, an anticlinal culmination is formed by progressive gain of structural elevation, and excision updip of the culmination axis produces a stacked series of progressively younger, structurally higher detachment faults. The excision model of *Lister and Davis* [1989], as applied to the Grant Range, explains the synextensional growth of the structural culmination, the progressive folding and incision over the top of the culmination axis, and the bottom-to-top order of emplacement and upward shallowing dip angle of faults in the imbricate stack.

However, the apparent thrust relationships observed west of the culmination axis are not predicted by the original *Lister and Davis* [1989] model. We propose that this was the result of excision downdip of the culmination axis (Figure 11a). As an active detachment crossed the culmination axis, the difference in dip angle between the updip and downdip segments was significant enough that excision splays branched structurally upward downdip of the axis, producing apparent thrust relationships. This served as a mechanism to minimize the difference in dip angle of an active detachment surface across the culmination. The sharp axis of the Grant Range culmination, which contrasts with the broad, domal culminations documented in several Cordilleran core complexes [e.g., *Gans and Miller*, 1983; *Spencer*, 1984; *Lister and Davis*, 1989], was an additional factor that promoted excision downdip of the culmination axis.

A kinematic model illustrating development of the set 1 fault system is shown in Figure 11b, in the form of schematic, incrementally deformed cross sections. Key elements illustrated in the model include growth of a stationary culmination as an isostatic response to progressive tectonic thinning, bottom-to-top construction of the imbricate stack through progressive rotation and excision updip of the culmination axis, and excision producing apparent thrust relationships downdip of the culmination axis.

6.2. Comparison to Geometric Models for Core Complex Detachment Systems

The geometry and kinematics of the Grant Range detachment system are best compared to models proposed for detachment systems in metamorphic core complexes. However, as a structural case study, the Grant Range is unique in several important ways, two of which are discussed here.

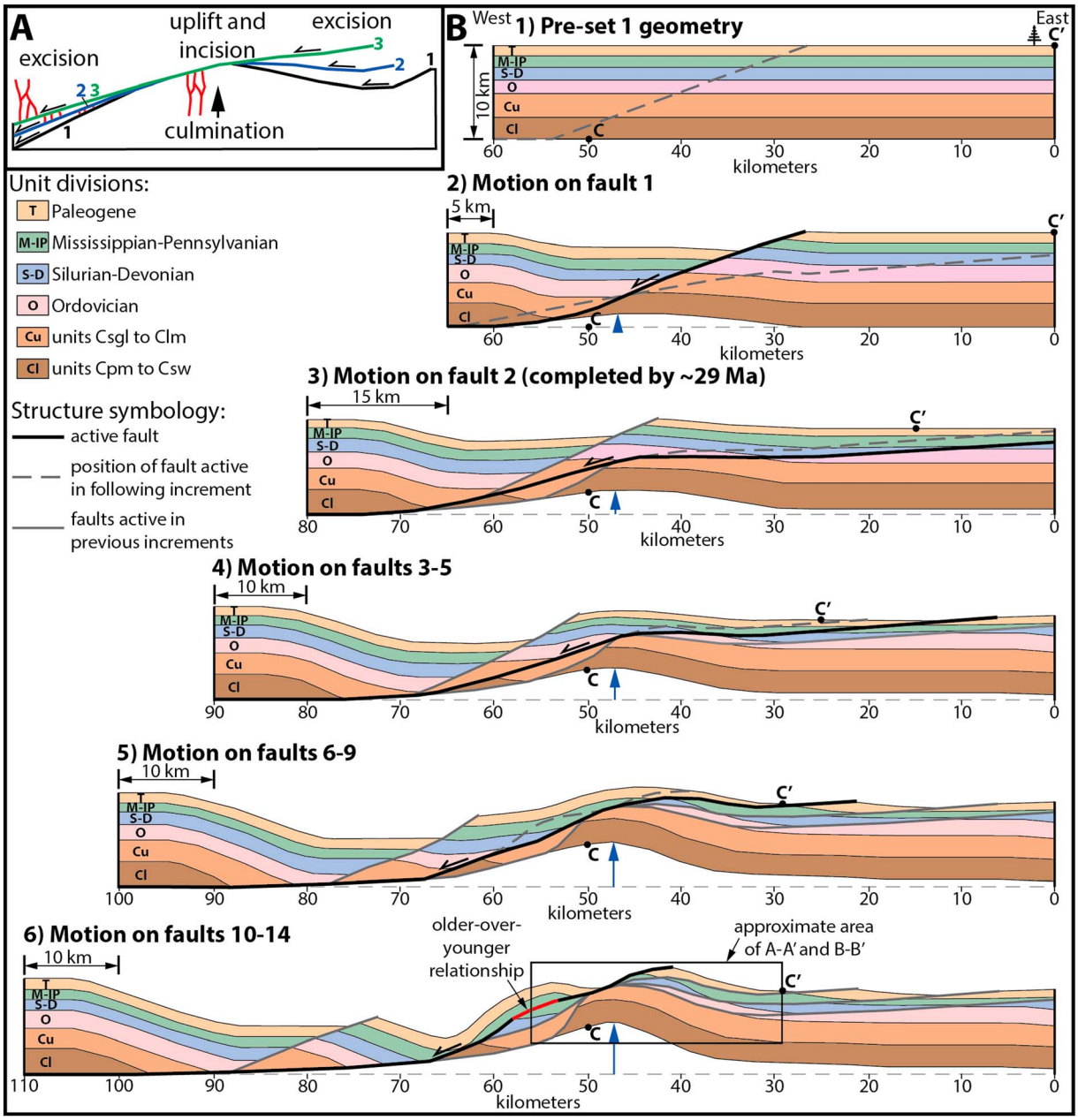

Figure 11. (a) Diagram illustrating progressive growth of stationary culmination, with uplift and incision above axial zone and excision updip and downdip of axial zone [modified from *Lister and Davis*, 1989]. Faults are numbered in relative order of emplacement and do not correspond to specific numbered detachment faults in the study area. (b) Schematic cross sections showing incremental development of set 1 fault system in the Grant Range. Stratigraphic thicknesses and horizontal distances approximate Figure 10. Increments 4–6 are meant to represent cumulative offset on multiple faults, which are simplified as one fault in each increment. Points C and C′ approximate the fixed and mobile points used to estimate set 1 extension on cross sections A–A′ and B–B′. Increments 5 and 6 show excision downdip of culmination axis producing an older-over-younger relationship.

6.2.1. Style of Upper Plate Extension Above the Master Detachment

Many classic models of Cordilleran core complexes [e.g., *Gans and Miller*, 1983; *Spencer*, 1984; *Lister and Davis*, 1989] are presented as a two-part division of an internally extended "upper plate" above a master, low-angle detachment fault. End-member geometric styles of upper plate extension include arrays of listric normal faults that rotate intervening fault blocks by reverse drag and sole into the master detachment [e.g., *Davis et al.*, 1980], or closely spaced arrays of high-angle normal faults, which rotate domino-style with progressive extension [e.g., *Proffett*, 1977; *Chamberlin*, 1983]. In the domino-style model, as older faults rotate to shallow dips, they become inactive, and a new generation of faults forms; this

geometry is exemplified by the upper plate of the Northern Snake Range décollement in eastern Nevada [*Gans and Miller*, 1983; *Gans et al*., 1985].

In comparison, the Grant Range detachment system exhibits a significantly different extension style. All set 1 faults show evidence of being active at initially low dip angles (≤15°) and traversed the entire upper ~8–10 km of the crust at these low dip angles. Set 1 faults merge westward into a basal footwall level shared by faults 10 and 12, which is analogous to the master detachment level defined in core complex models. However, the style of normal faulting recorded in all allochthonous rocks above this master detachment level is characterized by low-angle excision that yielded stacked sets of thin, fault-bound sheets. At all observed structural levels, including within Mississippian, Pennsylvanian, and Paleogene rocks that represent the upper few kilometers of the crust, there are no preserved high-angle (≥30°) or listric normal faults that internally deform these thin, elongate sheets. This contrasts with other extensional systems that record excision, including the Whipple Mountains detachment system in California [*Lister and Davis*, 1989; *Yin and Dunn*, 1992] and the Bannock detachment system in Idaho [*Carney and Janecke*, 2005], which exhibit multiple, high-angle, upper plate faults that truncate into a basal detachment and are interpreted as the result of excision of the basal part of listric fault blocks.

6.2.2. Long-Duration Site of Isostatic Rebound: A "Fixed Hinge"

Many field- and model-based studies have documented denudation-induced doming of large-offset normal fault systems during extension [e.g., *Spencer*, 1984; *Buck*, 1988; *Wernicke and Axen*, 1988; *Lister and Davis*, 1989]. Several studies have proposed a "rolling hinge" mechanism, in which the locus of isostatic uplift migrates progressively downdip, following retreat of the hanging wall. Variations of this model range from doming of detachment faults that originated at low dip angles [*Spencer*, 1984] to normal faults that originated at a steep angle through the seismogenic crust and were rotated to a shallow dip as an isostatic response to denudation [*Buck*, 1988; *Wernicke and Axen*, 1988].

The Grant Range detachment system displays compelling evidence for a synextensional isostatic "hinge," in the form of a structural culmination. However, several field observations, including multiple excision faults branching from the culmination axis, increased vertical thinning with proximity to the axis, and progressively increasing folding and incision over the axial zone, indicate that the culmination was a long-lived, stationary zone of rock uplift for the duration of set 1 extension, as opposed to a hinge that migrated westward with progressive extension. Growth of this "fixed hinge" rotated faults from primary dip angles of ≤15°W to progressively shallower angles, including back rotation of the oldest faults in the imbricate stack to dips as high as ~20°E. This is similar to the typical ≤30° of synextensional rotation documented in field-based studies of several Cordilleran detachment fault systems [*Axen and Bartley*, 1997].

The lack of hinge migration in the down-transport direction was likely aided by excision downdip of the culmination axis, which resulted in local stratigraphic repetition and therefore less tectonic denudation than the axial zone. Therefore, the Grant Range illustrates a unique example in which increased denudation, incision, and erosion over the axial zone created a positive feedback process that continued to spatially focus uplift, thereby favoring a fixed hinge. The end product is a low-wavelength, synextensional culmination that comes to a sharp apex, which differs from the broad domes produced in rolling hinge models [e.g., *Spencer*, 1984].

6.3. The Grant Range Detachment System in the Context of Paleogene, Low-Angle Extension Within the Cordilleran Retroarc Plateau

The formation of brittle normal faults at primary low dip angles remains a debated mechanical problem [e.g., *Axen*, 2007]. In many cases, unique boundary conditions are invoked, including tectonic scenarios that rotate upper crustal stress fields to favorable orientations [e.g., *Dalmayrac and Molnar*, 1981; *Burchfiel and Royden*, 1985; *Spencer and Chase*, 1989; *Yin*, 1989; *Westaway*, 1999] or assumption that normal faults are frictionally weaker than predicted by fault mechanical theory [e.g., *Hubbert and Rubey*, 1959; *Tong and Yin*, 2011; *Tong*, 2014].

In the eastern Great Basin, early postorogenic extension within the Cordilleran retroarc plateau was in many places accommodated by low-angle faulting, including Paleogene tectonic denudation of metamorphic core complexes [e.g., *Dickinson*, 2006]. Many have documented that core complex extension was closely associated in space and time with the Eocene-Oligocene Great Basin ignimbrite flare-up [e.g., *Zoback et al*., 1981; *Gans et al*., 1989; *Armstrong and Ward*, 1991; *Dickinson*, 2002], a north-south sweep of silicic magmatism

interpreted as the surface expression of rollback of the subducting Laramide slab [e.g., *Dickinson and Snyder*, 1978; *Humphreys*, 1995]. This early, postorogenic extension was promoted by several factors, including slab rollback reducing interplate shear, the presence of crust thickened by Cordilleran contractional deformation, and crustal heating through input of mantle-derived magmas [e.g., *Dickinson*, 1991, 2006]. Field- and modeling-based studies have shown that Cordilleran core complex extension was accompanied by lower crustal flow [*Gans and Miller*, 1983; *Gans*, 1987; *Yin*, 1989; *Wernicke*, 1992; *Harry et al*., 1993; *MacCready et al*., 1997], and shear traction applied to the base of the brittle crust during lower crustal flow is interpreted to have rotated principal stresses in the upper crust to favorable orientations for Paleogene low-angle detachment faulting [*Yin*, 1989; *Harry et al*., 1993; *Westaway*, 1999]. As the lower crust of the retroarc region thinned and cooled with additional extension, ductile flow became inhibited, which likely contributed to the overall change in extension style to the high-angle, block-style normal faulting that typifies Neogene Basin and Range extension [*Harry et al*., 1993].

The duration of detachment faulting in the Grant Range is not precisely constrained. However, based on geochronology and crosscutting relations described above, extension must have been underway by ~29 Ma, and the lack of differential tilting between ~32 to 34 Ma volcanic rocks and underlying Paleogene and Paleozoic rocks indicates that extension most likely initiated after ~32 Ma. This Late Oligocene initiation was approximately coeval with the ~30–35 Ma sweep of ignimbrite flare-up magmatism through this region of Nevada [*Dickinson*, 2006; *Henry and John*, 2013]. Therefore, the Grant Range detachment system can be placed in the temporal context of the episode of Paleogene, core complex-dominated extension within the Cordilleran retroarc plateau [e.g., *Dickinson*, 2006] and represents one of the youngest known localities of extension during post-Laramide slab rollback. Therefore, after the models of *Yin* [1989], *Harry et al*. [1993], and *Westaway* [1999], low-angle detachment faulting in the Grant Range is interpreted to have been favored by rotation of the upper crustal stress field as a result of shear traction imparted by lower crustal flow.

Acknowledgments

This work was funded by the USGS Statemap program, agreement #G13AC00235. The authors would like to thank Chris Henry, who collected the $^{40}Ar/^{39}Ar$ date for sample GR63, with assistance from Bill McIntosh at the New Mexico Geochronology Research Laboratory. Conversations with several researchers, including Karen Lund, Sue Beard, Joe Colgan, Jim Faulds, and Don French, contributed to ideas presented here. Comments from editor J. Geissman, associate editor M. Oskin, and two anonymous reviewers significantly improved this manuscript. GIS data files of the geologic map (Figure 4) are available upon request from the corresponding author. All other supporting data for this research are included in the manuscript and supporting information.

References

Abers, G. A. (2001), Evidence for seismogenic normal faults at shallow dips in continental rifts, in *Non-volcanic Rifting of Continental Margins: A Comparison of Evidence From Land and Sea*, edited by R. C. L. Wilson et al., *Geol. Soc. London Spec. Publ.*, *187*, 305–318.

Allmendinger, R. W. (1992), Fold and thrust tectonics of the western United States exclusive of the accreted terranes, in *The Cordilleran Orogen: Conterminous U.S.*, *Geol. Soc. Am., Geol. North Am*., vol. G-3, edited by B. C. Burchfiel et al., pp. 583–607, Geol. Soc. of Am., Boulder, Colo.

Anderson, E. M. (1942), *The Dynamics of Faulting and Dyke Formation With Application to Britain*, vol. 191, Oliver and Boyd, Edinburgh.

Armstrong, R. L. (1968), Sevier orogenic belt in Nevada and Utah, *Geol. Soc. Am. Bull.*, *79*, 429–458.

Armstrong, R. L., and P. Ward (1991), Evolving geographic patterns of Cenozoic magmatism in the North American Cordillera: The temporal and spatial association of magmatism and metamorphic core complexes, *J. Geophys. Res.*, *96*, 13,201–13,224, doi:10.1029/91JB00412.

Atwater, T. (1970), Implications of plate tectonics for the Cenozoic evolution of North America, *Geol. Soc. Am. Bull.*, *81*, 3513–3536.

Axen, G. J. (2004), Mechanics of low-angle normal faults, in *Rheology and Deformation in the Lithosphere at Continental Margins*, edited by G. Karner et al., pp. 46–91, Columbia Univ. Press, New York.

Axen, G. J. (2007), Research focus: Significance of large-displacement low-angle normal faults, *Geology*, *35*, 287–288.

Axen, G. J., and J. M. Bartley (1997), Field test of rolling hinges: Existence, mechanical types, and implications for extensional tectonics, *J. Geophys. Res.*, *102*, 20,515–20,537, doi:10.1029/97JB01355.

Axen, G. J., W. J. Taylor, and J. M. Bartley (1993), Space–time patterns and tectonic controls of Tertiary extension and magmatism in the Great Basin of the western United States, *Geol. Soc. Am. Bull.*, *105*, 56–76, doi:10.1130/0016-7606(1993)105<0056:STPATC>2.3.CO;2.

Bartley, J. M., and G. C. Gleason (1990), Tertiary normal faults superimposed on Mesozoic thrusts, Quinn Canyon and Grant Ranges, Nye County, Nevada, in *Basin and Range Extensional Tectonics Near the Latitude of Las Vegas Nevada*, edited by B. P. Wernicke, *Mem. Geol. Soc. Am.*, *176*, 195–212.

Barton, M. D. (1990), Cretaceous magmatism, metamorphism, and metallogeny in the east-central Great Basin, in *The Nature and Origin of Cordilleran Magmatism*, edited by J. L. Anderson, *Mem. Geol. Soc. Am.*, *174*, 283–302.

Best, M. G., and E. H. Christiansen (1991), Limited extension during peak Tertiary volcanism, Great Basin of Nevada and Utah, *J. Geophys. Res.*, *96*, 13,509–13,528, doi:10.1029/91JB00244.

Boillot, G., and N. Froitzheim (2001), Non-volcanic rifted margins, continental break-up and the onset of sea-floor spreading: Some outstanding questions, in *Non-volcanic Rifting of Continental Margins: A Comparison of Evidence From Land and Sea*, edited by R. C. L. Wilson et al., *Geol. Soc. London Spec. Publ.*, *187*, 9–30.

Brady, R., B. Wernicke, and J. Fryxell (2000), Kinematic evolution of a large-offset continental normal fault system, South Virgin Mountains, Nevada, *Geol. Soc. Am. Bull.*, *112*, 1375–1397.

Buck, W. R. (1988), Flexural rotation of normal faults, *Tectonics*, *7*, 959–973, doi:10.1029/TC007i005p00959.

Burchfiel, B. C., and L. H. Royden (1985), North-south extension within the convergent Himalayan region, *Geology*, *13*, 679–682, doi:10.1130/0091-7613(1985)13<679:NEWTCH>2.0.CO;2.

Burchfiel, B. C., C. Zhiliang, K. V. Hodges, L. Yuping, L. H. Royden, D. Changrong, and X. Jiene (1992), The south Tibetan detachment system, Himalayan orogen: Extension contemporaneous with and parallel to shortening in a collisional mountain belt, *Geol. Soc. Am. Spec. Pap.*, *269*, 41.

Camilleri, P. A. (1992), Extensional geometry of a part of the northwestern flank of the northern Grant Range, Nevada: Inferences on its evolution, *Mt. Geol.*, *29*, 75–84.

Camilleri, P. A. (2013), Geologic map and structure of the west-central part of the Grant Range, Nye County, Nevada, *Geol. Soc. Am. Dig. Map Chart Ser.*, *14*, 25, doi:10.1130/2013.DMCH014.
Camilleri, P. A., and K. R. Chamberlain (1997), Mesozoic tectonics and metamorphism in the Pequop Mountains and Wood Hills region, northeast Nevada: Implications for the architecture and evolution of the Sevier orogen, *Geol. Soc. Am. Bull.*, *109*, 74–94, doi:10.1130/0016-7606(1997)109<0074:MTAMIT>2.3.CO;2.
Carney, S. M., and S. U. Janecke (2005), Excision and the original low dip of the Miocene-Pliocene Bannock detachment system, SE Idaho: Northern cousin of the Sevier Desert detachment?, *Geol. Soc. Am. Bull.*, *117*, 334–353, doi:10.1130/B25428.1.
Cashman, P. H., D. E. Villa, W. J. Taylor, V. I. Davydov, and J. H. Trexler Jr. (2011), Late Paleozoic contractional and extensional deformation at Edna Mountain, Nevada, *Geol. Soc. Am. Bull.*, *123*, 651–668, doi:10.1130/B30247.1.
Cebull, S. E. (1970), Bedrock geology and orogenic succession in southern Grant Range, Nye County, Nevada, *Am. Assoc. Petrol. Geol. Bull.*, *54*, 1828–1842.
Chamberlin, R. M. (1983), Cenozoic domino-style crustal extension in the Lemitar Mountains, New Mexico: A summary, in *Guidebook, 34th Field Conference, Socorro Region II*, *New Mexico Geological Society*, vol. 34, edited by C. E. Chapin and J. F. Callender, pp. 111–118, New Mexico Geol. Soc., Socorro, New Mexico.
Colgan, J. P., and C. D. Henry (2009), Rapid middle Miocene collapse of the Sevier orogenic plateau in north-central Nevada, *Int. Geol. Rev.*, *51*, 920–961.
Collettini, C., and R. H. Sibson (2001), Normal faults, normal friction?, *Geology*, *29*, 927–930, doi:10.1130/0091-7613(2001)029<0927:NFNF>2.0.CO;2.
Coney, P. J., and T. J. Harms (1984), Cordilleran metamorphic core complexes: Cenozoic extensional relics of Mesozoic compression, *Geology*, *12*, 550–554, doi:10.1130/0091-7613(1984)12<550:CMCCCE>2.0.CO;2.
Crafford, A. E. J. (2007), *Geologic Map of Nevada*, *U.S. Geol. Surv., Data Ser.*, vol. 249, 46 pp., 1 plate.
Crittenden, M. D., Jr., P. J. Coney, and G. H. Davis (1980), Cordilleran metamorphic core complexes, *Geol. Soc. Am. Mem.*, *153*, 490.
Dalmayrac, B., and P. Molnar (1981), Parallel thrust and normal faulting in Peru and the constraints on the state of stress, *Earth Planet. Sci. Lett.*, *55*, 473–481, doi:10.1016/0012-821X(81)90174-6.
Davis, G. A., J. L. Anderson, E. G. Frost, and T. J. Shakelford (1980), Mylonitization and detachment faulting in the Whipple-Buckskin-Rawhide Mountains terrane, southeastern California, and western Arizona, *Mem. Geol. Soc. Am.*, *153*, 79–130.
Davis, G. H., and P. J. Coney (1979), Geologic development of Cordilleran metamorphic core complexes, *Geology*, *7*, 120–124, doi:10.1130/0091-7613(1979)7<120:GDOTCM>2.0.CO;2.
DeCelles, P. G. (2004), Late Jurassic to Eocene evolution of the Cordilleran thrust belt and foreland basin system, western U.S.A., *Am. J. Sci.*, *304*, 105–168, doi:10.2475/ajs.304.2.105.
Dickinson, W. R. (1991), Tectonic setting of faulted Tertiary strata associated with the Catalina core complex in southern Arizona, *Geol. Soc. Am. Spec. Pap.*, *264*, 106.
Dickinson, W. R. (2002), The Basin and Range province as a composite extensional domain, *Int. Geol. Rev.*, *44*, 1–38, doi:10.2747/0020-6814.44.1.1.
Dickinson, W. R. (2006), Geotectonic evolution of the Great Basin, *Geosphere*, *2*, 353–368, doi:10.1130/GES00054.1.
Dickinson, W. R., and W. S. Snyder (1978), Plate tectonics of the Laramide orogeny, in *Laramide Folding Associated With Basement Block Faulting in the Western United States*, edited by V. Matthews III, *Mem. Geol. Soc. Am.*, *151*, 355–366.
Druschke, P., A. D. Hanson, M. L. Wells, T. Rasbury, D. F. Stockli, and G. Gehrels (2009a), Synconvergent surface-breaking normal faults of Late Cretaceous age within the Sevier hinterland, east-central Nevada, *Geology*, *37*, 447–450, doi:10.1130/G25546A.1.
Druschke, P., A. D. Hanson, and M. L. Wells (2009b), Structural, stratigraphic, and geochronologic evidence for extension predating Palaeogene volcanism in the Sevier hinterland, east-central Nevada, *Int. Geol. Rev.*, *51*, 743–775.
Elliott, D. (1983), The construction of balanced cross-sections, *J. Struct. Geol.*, *5*, 101.
Fouch, T. D. (1979), Character and paleogeographic distribution of Upper Cretaceous(?) and Paleogene nonmarine sedimentary rocks in east-central Nevada, in *Society of Economic Petrologists and Mineralogists Pacific Coast Paleogeography Symposium*, vol. 3, pp. 97–112, Rocky Mountain Assoc. of Petrol. Geol. and Utah Geol. Assoc., Denver, Colo.
French, D. E. (1993), Debris slides of the Railroad Valley area, Nye County, Nevada: Yet another interpretation of Grant Canyon and Bacon Flat fields (abs.), *Am. Assoc. Petrol. Geol. Bull.*, *77*, –1448.
Fryxell, J. E. (1988), Geologic map and description of stratigraphy and structure of the west-central Grant Range, Nye County, Nevada, *Geol. Soc. Am. Map Chart Ser.*, MCH064, 16 p.
Gans, P. B. (1987), An open-system, two-layer crustal stretching model for the eastern Great Basin, *Tectonics*, *6*, 1–12, doi:10.1029/TC006i001p00001.
Gans, P. B., and E. L. Miller (1983), Style of mid-Tertiary extension in east-central Nevada, in *Geologic Excursions in the Overthrust Belt and Metamorphic Core Complexes of the Intermountain Region*, *Utah Geol. Min. Surv. Spec. Study*, edited by K. D. Gurgel, pp. 107–160, Utah Geol. and Miner. Surv. Spec. Study, Salt Lake City, Utah.
Gans, P. B., E. L. Miller, J. McCarthy, and M. L. Ouldcott (1985), Tertiary extensional faulting and evolving ductile-brittle transition zones in the northern Snake Range and vicinity: New insights from seismic data, *Geology*, *13*, 189–193.
Gans, P. B., G. A. Mahood, and E. Schermer (1989), Synextensional magmatism in the Basin and Range province: A case study from the eastern Great Basin, *Geol. Soc. Am. Spec. Pap.*, *233*, 53.
Gans, P. B., E. Seedorff, P. L. Fahey, R. W. Hasler, D. J. Maher, R. A. Jeanne, and S. A. Shaver (2001), Rapid Eocene extension in the Robinson district, White Pine County, Nevada: Constraints for $^{40}Ar/^{39}Ar$ dating, *Geology*, *29*, 475–487.
Hansen, L. N., M. J. Cheadle, B. E. John, S. M. Swapp, H. J. B. Dick, B. E. Tucholke, and M A. Tivey (2013), Mylonitic deformation at the Kane oceanic core complex: Implications for the rheological behavior of oceanic detachment faults, *Geochem. Geophys. Geosyst.*, *8*, 3085–3108, doi:10.1002/ggge.20184.
Harris, A. G., B. R. Wardlaw, C. C. Rust, and G. K. Merrill (1980), Maps for assessing thermal maturity (conodont color alteration index maps) in Ordovician through Triassic rocks in Nevada and Utah and adjacent parts of Idaho and California, *U.S. Geol. Surv. Misc. Invest. Ser.*, Map I-1249, 2 sheets.
Harry, D. L., D. S. Sawyer, and W. F. Leeman (1993), The mechanics of continental extension in western North America: Implications for the magmatic and structural evolution of the Great Basin, *Earth Planet. Sci. Lett.*, *117*, 59–71, doi:10.1016/0012-821X(93)90117-R.
Henry, C. D., and D. A. John (2013), Magmatism, ash-flow tuffs, and calderas of the ignimbrite flareup in the western Nevada volcanic field, Great Basin, USA, *Geosphere*, *9*, 951–1008, doi:10.1130/GES00867.1.
Hess, R. H., S. P. Fitch, and S. N. Warren (2004), Nevada oil and gas well database, *Nev. Bur. Mines Geol. Open File Rep.* 04-1, 4 pp.
Hodges, K. V., and J. D. Walker (1992), Extension in the Cretaceous Sevier orogen, North American Cordillera, *Geol. Soc. Am. Bull.*, *104*, 560–569, doi:10.1130/0016-7606(1992)104<0560:EITCSO>2.3.CO;2.

Horton, B. K., and J. G. Schmitt (1998), Development and exhumation of a Neogene sedimentary basin during extension, east-central Nevada, *Geol. Soc. Am. Bull.*, *110*, 163–172.
Hubbert, M. K., and W. W. Rubey (1959), Role of fluid pressure in mechanics of overthrust faulting 1. Mechanics of fluid-filled porous solids and its application to overthrust faulting, *Geol. Soc. Am. Bull.*, *70*, 115–166, doi:10.1130/0016-7606(1959)70[115:ROFPIM]2.0.CO;2.
Hulen, J. B., F. Goff, J. R. Ross, L. C. Bortz, and S. R. Bereskin (1994), Geology and geothermal origin of Grant Canyon and Bacon Flat oil fields, Railroad Valley, Nevada, *Am. Assoc. Petrol. Geol. Bull.*, *78*, 596–623.
Humphreys, E. D. (1995), Post-Laramide removal of the Farallon slab, western United States, *Geology*, *23*, 987–990.
Hyde, J. H., and G. W. Huttrer (1970), Geology of the central Grant Range, Nevada, *Am. Assoc. Petrol. Geol. Bull.*, *54*, 503–521.
Jackson, J. A., and N. J. White (1989), Normal faulting in the upper continental crust: Observations from regions of active extension, *J. Struct. Geol.*, *11*, 15–36, doi:10.1016/0191-8141(89)90033-3.
Johnson, E. H. (1993), A look at Bacon Flat, Grant Canyon oil fields of Railroad Valley, Nevada, *Oil Gas J.*, *91*, 64–68.
Kapp, P., M. Taylor, D. Stockli, and L. Ding (2008), Development of active low-angle normal fault systems during orogenic collapse: Insight from Tibet, *Geology*, *36*, 7–10, doi:10.1130/G24054A.1.
Kellogg, H. E. (1963), Paleozoic stratigraphy of the southern Egan Range, Nevada, *Geol. Soc. Am. Bull.*, *74*, 685–708.
Kellogg, H. E. (1964), Cenozoic stratigraphy of the southern Egan Range, east-central Nevada, *Geol. Soc. Am. Bull.*, *75*, 949–968.
Kleimhampl, F. J., and J. L. Ziony (1985), Geology of northern Nye County, Nevada, *Nev. Bur. Mines Bull.*, *99A*, 171.
Konighshof, P. (2003), Conodont deformation patterns and textural alteration in Paleozoic conodonts: Examples from Germany and France, *Paleobiodiv. Paleoenvir.*, *83*, 149–156.
Leeder, M. R., and R. L. Gawthorpe (1987), Sedimentary models for extensional tilt-block/half-graben basins, in *Continental Extensional Tectonics*, edited by M. P. Coward, J. F. Dewey, and P. L. Hancock, *Geol. Soc. Am. Spec. Publ.*, *28*, 139–152.
Lewis, C. J., B. P. Wernicke, J. Selverstone, and J. M. Bartley (1999), Deep burial of the footwall of the northern Snake Range decollement, Nevada, *Geol. Soc. Am. Bull.*, *111*, 39–51.
Lister, G. S., and G. A. Davis (1989), The origin of metamorphic core complexes and detachment faults during Tertiary continental extension in the northern Colorado River region, U.S.A., *J. Struct. Geol.*, *11*, 65–94.
Lister, G. S., M. A. Etheridge, and P. A. Symonds (1986), Detachment faulting and the evolution of passive continental margins, *Geology*, *14*, 246–250, doi:10.1130/0091-7613(1986)14<246:DFATEO>2.0.CO;2.
Livaccari, R. F., J. W. Geissman, and S. J. Reynolds (1995), Large-magnitude extensional deformation in the South Mountains metamorphic core complex, Arizona: Evaluation with paleomagnetism, *Geol. Soc. Am. Bull.*, *107*, 877–894.
Long, S. P. (2012), Magnitudes and spatial patterns of erosional exhumation in the Sevier hinterland, eastern Nevada and western Utah, U.S.A.: Insights from a Paleogene paleogeologic map, *Geosphere*, *8*, 881–901, doi:10.1130/GES00783.1.
Long, S. P. (2014), Preliminary geologic map of Heath Canyon, central Grant Range, Nye County, Nevada, *Nev. Bur. Mines Geol. Open File Rep.* 14-6, 1:24,000-scale, 1 plate, 4 pp.
Long, S. P. (2015), An upper-crustal fold province in the hinterland of the Sevier orogenic belt, eastern Nevada, U.S.A.: A Cordilleran Valley and Ridge in the Basin and Range, *Geosphere*, *11*, 404–424, doi:10.1130/GES01102.1.
Long, S. P., C. D. Henry, J. L. Muntean, G. P. Edmondo, and E. J. Cassel (2014), Early Cretaceous construction of a structural culmination, Eureka, Nevada, U.S.A.: Implications for out-of-sequence deformation in the Sevier hinterland, *Geosphere*, *10*, 505–553, doi:10.1130/GES00997.1.
Long, S. P., S. N. Thomson, P. W. Reiners, and R. V. Di Fiori (2015), Synorogenic extension localized by upper-crustal thickening: An example from the Late Cretaceous Nevadaplano, *Geology*, *43*, 351–354, doi:10.1130/G36431.1.
Lund, K., J. T. Nash, L. S. Beard, H. R. Blank Jr., and S. E. Tuftin (1987), Mineral resources of the Blue Eagle Wilderness Study Area, Nye County, Nevada, *U.S. Geol. Soc. Am. Bull.* 1731-D, 19 pp.
Lund, K., L. S. Beard, H. R. Blank Jr., A. H. Hofstra, and M. M. Hamilton (1988), Mineral resources of the Riordans Well Wilderness Study Area, Nye County, Nevada, *U.S. Geol. Soc. Am. Bull.* 1731-H, 16 pp.
Lund, K., S. L. Beard, and W. J. Perry (1993), Relation between extensional geometry of the northern Grant Range and oil occurrences in Railroad Valley, east-central Nevada, *Am. Assoc. Petrol. Geol. Bull.*, *77*, 945–962, doi:10.1306/BDFF8DA8-1718-11D7-8645000102C1865D.
Lund, K., S. L. Beard, and J. P. Colgan (2014), Shrimp U-Pb dating of zircon reveals Oligocene, Late Cretaceous, and Late Jurassic ages in Troy granite, east-central Nevada, *Geol. Soc. Am. Abstr. Prog.*, *46*, 30.
MacCready, T., A. W. Snoke, J. E. Wright, and K. A. Howard (1997), Mid-crustal flow during Tertiary extension in the Ruby Mountains core complex, Nevada, *Geol. Soc. Am. Bull.*, *109*, 1576–1594, doi:10.1130/0016-7606(1997)109<1576:MCFDTE>2.3.CO;2.
McCutcheon, T. J., and W. D. Zogg (1994), Structural geology of the Grant Canyon-Bacon Flat field area, Nye County, Nevada: Implications for hydrocarbon exploration in the Great Basin, in *Oil Fields of the Great Basin*, edited by R. A. Schalla and E. H. Johnson, *Nev. Pet. Soc. Spec. Publ.*, 201–226.
McGrew, A. J., M. T. Peters, and J. E. Wright (2000), Thermobarometric constraints on the tectonothermal evolution of the East Humboldt Range metamorphic core complex, Nevada, *Geol. Soc. Am. Bull.*, *112*, 45–60.
Miller, D. M., and T. D. Hoisch (1995), Jurassic tectonics of northeastern Nevada and northwestern Utah from the perspective of barometric studies, *Geol. Soc. Am. Spec. Pap.*, *299*, 267–294.
Miller, E. L., and P. B. Gans (1989), Cretaceous crustal structure and metamorphism in the hinterland of the Sevier thrust belt, western U.S. Cordillera, *Geology*, *17*, 59–62, doi:10.1130/0091-7613(1989)017<0059:CCSAMI>2.3.CO;2.
Miller, E. L., P. B. Gans, J. E. Wright, and J. F. Sutter (1988), Metamorphic history of the east-central Basin and Range province: Tectonic setting and relationship to magmatism, in *Metamorphism and Crustal Evolution, Western Conterminous United States*, vol. 7, edited by W. G. Ernst, pp. 649–682, Prentice-Hall, Englewood Cliffs, N. J.
Moores, E. M., R. B. Scott, and W. W. Lumsden (1968), Tertiary tectonics of the White Pine-Grant Range, east-central Nevada, and some regional implications, *Geol. Soc. Am. Bull.*, *79*, 1703–1726.
Nur, A., H. Ron, and O. Scotti (1986), Fault mechanics and the kinematics of block rotations, *Geology*, *14*, 746–749, doi:10.1130/0091-7613(1986)14<746:FMATKO>2.0.CO;2.
Peterson, J. A. (1994), Regional geology and paleotectonic development of the Railroad Valley area, in *Oil Fields of the Great Basin*, edited by R. A. Schalla and E. H. Johnson, *Nev. Pet. Soc. Spec. Publ.*, 15–40.
Poole, F. G., and C. A. Sandberg (1977), Mississippian paleogeography and tectonics of the western United States, in *Paleozoic Paleogeography of the Western United States, Soc. Econ. Paleont. Mineral. Pacific Section Pacific Coast Paleogeography Symposium*, vol. 1, edited by J. H. Stewart, C. H. Stevens, and A. E. Fritsche, pp. 67–85, Soc. Econ. Paleont. Mineral, Tulsa, Okla.
Proffett, J. M., Jr. (1977), Cenozoic geology of the Yerington District, Nevada, and implications for nature and origin of Basin and Range faulting, *Geol. Soc. Am. Bull.*, *88*, 247–266, doi:10.1130/0016-7606(1977)88<247:CGOTYD>2.0.CO;2.

Selverstone, J. (1988), Evidence for east-west crustal extension in the eastern Alps: Implications for the unroofing history of the Tauern window, *Tectonics*, *7*, 87–105, doi:10.1029/TC007i001p00087.
Speed, R. C., and N. Sleep (1982), Antler orogeny and foreland basin: A model, *Geol. Soc. Am. Bull.*, *93*, 815–828.
Spencer, J. E. (1984), The role of tectonic denudation in the warping and uplift of low-angle normal faults, *Geology*, *12*, 95–98, doi:10.1130/0091-7613(1984)12<95:ROTDIW>2.0.CO;2.
Spencer, J. E., and C. G. Chase (1989), Role of crustal flexure in initiation of low-angle normal faults and implications for structural evolution of the Basin and Range province, *J. Geophys. Res.*, *94*, 1765–1775, doi:10.1029/JB094iB02p01765.
Stewart, J. H. (1980), Geology of Nevada: A discussion to accompany the Geologic Map of Nevada, *Nev. Bur. Mines Geol. Spec. Publ.*, *4*, 136.
Stewart, J. H. (1998), Regional characteristics, tilt domains, and extensional history of the later Cenozoic Basin and Range Province, western North America, in *Accommodation Zones and Transfer Zones: The Regional Segmentation of the Basin and Range Province*, edited by J. E. Faulds and J. H. Stewart, *Geol. Soc. Am. Spec. Pap.*, *323*, 47–74.
Stewart, J. H., and F. G. Poole (1974), Lower Paleozoic and uppermost Precambrian Cordilleran miogeocline, Great Basin, Western United States, in *Tectonics and Sedimentation*, edited by W. R. Dickinson, *Soc. Econ. Paleont. Mineral. Spec. Publ.*, *22*, 28–57.
Suppe, J. (1983), Geometry and kinematics of fault-bend folding, *Am. J. Sci.*, *283*, 684–721.
Taylor, W. J., J. M. Bartley, D. R. Lux, and G. J. Axen (1989), Timing of Tertiary extension in the Railroad Valley-Pioche transect, Nevada: Constraints from $^{40}Ar/^{39}Ar$ ages of volcanic rocks, *J. Geophys. Res.*, *94*, 7757–7774, doi:10.1029/JB094iB06p07757.
Taylor, W. J., J. M. Bartley, M. W. Martin, J. W. Geissman, J. D. Walker, P. A. Armstrong, and J. E. Fryxell (2000), Relations between hinterland and foreland shortening: Sevier orogeny, central North American Cordillera, *Tectonics*, *19*, 1124–1143, doi:10.1029/1999TC001141.
Tong, H. (2014), Modified Anderson model—Dynamics of brittle faulting, Abstract T31B-4604 presented at 2014 Fall Meeting, AGU, San Francisco, Calif.
Tong, H., and A. Yin (2011), Reactivation tendency analysis: A theory for predicting the temporal evolution of preexisting weakness under uniform stress state, *Tectonophysics*, *503*, 195–200, doi:10.1016/j.tecto.2011.02.012.
Trexler, J. H., Jr., P. H. Cashman, W. S. Snyder, and V. I. Davydov (2004), Upper Paleozoic tectonism in Nevada: Timing, kinematics, and tectonic significance, *Geol. Soc. Am. Bull.*, *116*, 525–538, doi:10.1130/B25295.1.
Tucholke, B. E., and J. Lin (1998), Megamullions and mullion structures defining oceanic metamorphic core complexes on the Mid-Atlantic Ridge, *J. Geophys. Res.*, *103*, 9857–9866, doi:10.1029/98JB00167.
Vandervoort, D. S., and J. G. Schmitt (1990), Cretaceous to early Tertiary paleogeography in the hinterland of the Sevier thrust belt, east-central Nevada, *Geology*, *18*, 567–570.
Wells, M. L., and T. D. Hoisch (2008), The role of mantle delamination in widespread Late Cretaceous extension and magmatism in the Cordilleran orogen, western United States, *Geol. Soc. Am. Bull.*, *120*, 515–530, doi:10.1130/B26006.1.
Wells, M. L., T. D. Hoisch, A. M. Cruz-Aribe, and J. D. Vervoort (2012), Geodynamics of synconvergent and tectonic mode switching: Constraints from the Sevier-Laramide orogen, *Tectonics*, *31*, TC1002, doi:10.1029/2011TC002913.
Wernicke, B. (1981), Low-angle normal faults in the Basin and Range Province: Nappe tectonics in an extending orogen, *Nature*, *291*, 645–648, doi:10.1038/291645a0.
Wernicke, B. (1995), Low-angle normal faults and seismicity: A review, *J. Geophys. Res.*, *100*, 20,159–20,174, doi:10.1029/95JB01911.
Wernicke, B., and G. J. Axen (1988), On the role of isostasy in the evolution of normal fault systems, *Geology*, *16*, 848–851, doi:10.1130/0091-7613(1988)016<0848:OTROII>2.3.CO;2.
Wernicke, B. P. (1992), Cenozoic extensional tectonics of the U.S. Cordillera, in *The Cordilleran Orogen: Conterminous U.S.*, *Geol. Soc. Am., Geol. North Am.*, vol. G-3, edited by B. C. Burchfiel, P. W. Lipman, and M. L. Zoback, pp. 553–581, Geol. Soc. of Am., Boulder, Colo.
Westaway, R. (1999), The mechanical feasibility of low-angle normal faulting, *Tectonophysics*, *308*, 407–443, doi:10.1016/S0040-1951(99)00148-1.
Yin, A. (1989), Origin of regional rooted low-angle normal faults: A mechanical model and its implications, *Tectonics*, *8*, 469–482, doi:10.1029/TC008i003p00469.
Yin, A., and J. F. Dunn (1992), Structural and stratigraphic development of the Whipple-Chemehuevi detachment fault system, southeastern California: Implications for the geometrical evolution of domal and basinal low-angle normal faults, *Geol. Soc. Am. Bull.*, *104*, 659–674, doi:10.1130/0016-7606(1992)104<0659:SASDOT>2.3.CO;2.
Zoback, M. L., R. E. Anderson, and G. A. Thompson (1981), Cenozoic evolution of the state of stress and style of tectonism of the Basin and Range province of the western United States, *Royal Soc. London Phil. Trans.*, *A300*, 407–434.